# FLEXIBLE LOW-COST WIRELESS TEMPERATURE SENSOR USING THERMORESPONSIVE Y5V CAPACITOR CHIPS

by

Ronish Patel

B.E., University of Pune, 2012

A THESIS SUBMITTED IN PARTIAL FULFILLMENT OF

THE REQUIREMENTS FOR THE DEGREE OF

MASTER OF APPLIED SCIENCE

in

THE FACULTY OF GRADUATE AND POSTDOCTORAL STUDIES

(Electrical and Computer Engineering)

THE UNIVERSITY OF BRITISH COLUMBIA

(Vancouver)

July 2019

The following individuals certify that they have read, and recommend to the Faculty of Graduate and Postdoctoral Studies for acceptance, a thesis/dissertation entitled:

**Flexible low-cost wireless temperature sensor using thermosresponsive Y5V capacitor chips**

submitted by    Ronish Patel                    in partial fulfillment of the requirements for

the degree of    Master of Applied Science

in                   Electrical & Computer Engineering

**Examining Committee:**

Kenichi Takahata
Supervisor

Shahriar Mirabbasi
Supervisory Committee Member

Shuo Tang
Additional Examiner

## Abstract

Temperature sensing is one of the most important abilities for monitoring and controlling thermal behaviors of target objects or environments, and the capability of its wireless reading largely expands the potential application areas. For example, biomedical and environmental applications are some of the promising areas for wireless temperature sensors.

The use of inductor-capacitor (LC) resonant-tank circuits in which the capacitance or the inductance is designed to vary with temperature, is an advantageous approach for wireless temperature sensing given its reliable frequency-based reading and no requirement for having internal power sources. Type Y5V multilayer dielectric capacitors, commercially available in low-cost (e.g., ~$0.01-0.1/chip) surface-mount chips, exhibit significant capacitance variations over a wide range of temperatures (-30 to +85 ℃). Such capacitors can serve as the sensing elements in LC-tank circuits for frequency-based wireless temperature reading.

The current work designs, fabricates, and demonstrates the first proof-of-concept device of a flexible wireless sensor that uses Y5V capacitor chips in combination with planar inductive coils microfabricated on thin polymer film, forming LC-tank-based devices. The physical flexibility and disposable nature of the devices makes them suitable for medical/healthcare applications, e.g., continuous remote monitoring of patient's body temperature and feedback control of clinical hyperthermia treatments for various cancer therapies.

This research presents the design, fabrication, and experimental validation of two prototype passive wireless LC temperature sensors of varying dimensions. The larger sized (20 mm$^2$) sensor

reported has a frequency response of 106-150KHz/°C and a resonant frequency of 152 MHz at room temperature. Whereas, the miniature (~6 mm$^2$) sized sensor reported demonstrates a frequency response of 77-119KHz/°C and a resonant frequency of 1.5 MHz at room temperature.

Moreover, a low-cost impedance analyzer is developed in this work. It consists of Raspi 3 host device and a Digilent PmodIA impedance analyzer has a low error of ~4% as compared to the Agilent network analyzer. The new analyzer is demonstrated and experimentally validated.

# Lay Summary

The primary objective of this research is to design flexible disposable low-cost passive wireless temperature sensors for wearable applications. During this work, commercial surface-mount device capacitors are studied and their applicability as temperature sensing elements are extensively investigated and reported. Two prototype inductive-capacitor resonator devices having larger ($20mm^2$) and smaller ($6\ mm^2$) dimensions are designed, developed, and experimentally validated. A novel low-cost inductor coil fabrication approach for them has been reported. The fabricated device requires no power to operate which increases its longevity, and its miniaturized dimensions provide ease of integration into wearable devices. With a change in temperature, the fabricated sensor device output frequency response changes; therefore, tracking its resonant frequency can provide the surface temperature profile of the sensor. An effort in developing a low-cost impedance analyzer is demonstrated it consists of a Raspi 3 as host device and a PmodIA impedance analyzer.

## Preface

This thesis is submitted for the degree of Master of Applied Science at The University of British Columbia. The research results presented in this thesis was guided by Professor Kenichi Takahata, in the Department of Electrical and Computer Engineering at University of British Columbia, between January 2017 and June 2019.

The technical and editing assistance was provided by Professor Kenichi Takahata. Moreover, Madesh Selvaraj provided the necessary skill transfer in the fabrication of planar inductance coils and capacitor bonding that is presented in Chapter 3. All of the work presented in this thesis was solely conducted by me. A journal paper based on the results presented in Chapter 3 is in preparation.

# Table of Contents

# List of Tables

# List of Figures

xi

## Acknowledgements

I offer my gratitude to the faculty, staff, and my fellow students in the ECE department at The University of British Columbia. I owe special thanks to Professor Kenichi Takahata for being my supervisor and my mentor in this field. I would also like to thank Jiaxu Chen, Madeshwaran Selvaraj, and Hashem Jayhooni for helping me with my research and providing the necessary training to use the advanced equipment which facilitated this research. I would like to thank the Faculty of Graduate and Postdoctoral Studies for their financial support. I wish to extend special thanks to my parents, friends, and my wife for supporting me during my study at UBC.

# Chapter 1: Introduction

## 1.1  Background and motivation

Temperatures sensing is one of the most important abilities in monitoring and controlling thermal behavior of target objects or environments, and the capability of its wireless reading largely expands the potential applications areas. For example, biomedical and environmental applications are some of the promising areas for the utilization of wireless temperature sensors [1][2]. The inductor-capacitor (LC) resonant circuit, in which the capacitance or inductance is designed to vary with temperature changes, is an advantageous approach for wireless temperature sensing. Such circuits offer reliable frequency based reading and have no requirements for internal power sources and physical connections. [1-3]. Passive LC sensors have two major advantages, miniature size and high longevity, which make them superior in sealed environments and biomedical implant applications. The simplicity of the LC sensor's structure also provides low cost manufacturing using batch processing. The rapid demand of Internet of Things (IoT) devices, mainly implantable sensors and wearable devices, has made LC passive wireless sensors a hot topic for research. In Chapter 2, various wireless passive temperature sensors using LC tank circuits are reviewed including their advantages and disadvantages. Since this research is mainly based on using commercial Y5V capacitors as the thermoresponsive element and a fixed inductor fabrication, the sensing mechanisms and novel low-cost fabrication techniques have been discussed in detail. The wireless sensing of temperature changes and monitoring the shift in resonance frequency are discussed and the need for low cost impedance analyzers for monitoring resonance frequency is demonstrated. The physical flexibly and disposable nature of devices that suit the medical/healthcare domain are identified, for example, the continuous remote monitoring of

patient body temperature as shown in Figure 1.1 and the feedback control of hyperthermia clinically used for various cancer therapies [1-8].
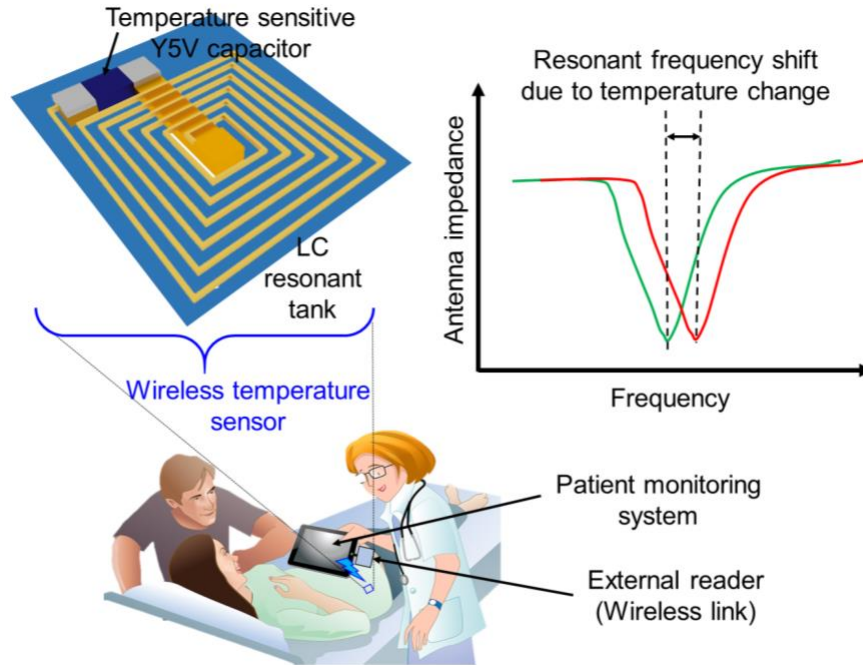


**Figure 1.1:Conceptual schematic of the wireless temperature sensor and its potential medical application**

## 1.2 Research contribution

To address the needs for low-cost, simple to fabricate temperature sensing devices and real time monitoring in the wearable sensor/healthcare sector, this thesis proposes a novel passive wireless temperature sensor and a low-cost sensing methodology. The aim is to develop, design, and characterize wireless passive temperature sensors and a portable low-cost impedance analyzer. The passive wireless sensor provides a unique resonance frequency at various temperature ranging from 30 °C to 70 °C. The sensor consists of micro-fabricated planar inductor coil and an integrated commercial Y5V capacitor. This device has a fixed inductance and temperature sensitive

2

capacitor. A novel fabrication technique using double sided copper clad layer is demonstrated; this technique is unlike the fabrication of previous devices such as micromachined inductive sensor using folded flex-circuit structures using single sided copper clad layer [23] [27]. The proposed technique minimizes the fabrication steps and clean room usage. Moreover, it involves the development of a portable low-cost impedance analyzer that consists of an analog device AD5933 and a Rasberrypi 3 module. The analyzer provides a high precision impedance converter system that can measure impedance ranging from 100$\Omega$ - 10M$\Omega$.

The goal of my research is to develop miniaturized temperature sensor and portable analyzer for monitoring the shift in resonance frequencies with changes in temperatures. This high precision impedance analyzer system can be used as a readout circuit for multiple LC sensors for applications such as capacitive and pressure sensing. Moreover, it also can prove advantageous for its foot-print and ease of use.

## 1.3 Overview of thesis

This thesis presents the design, development, and fabrication of flexible low-cost disposable wireless temperature sensor using a wet semiconductor fabrication process. Two different sizes (6 mm$^2$ and 20mm$^2$) of wireless temperature sensors are fabricated which have different frequency responses. Chapter 2 reviews the state-of-the-art wireless temperature sensing technologies for biomedical implants/wearable sensors. These technologies are briefly explained along with their limitations. Chapter 3 describes the characterization of the temperature sensing Y5V capacitor and explains how it can be useful for wireless temperature sensing applications. Chapter 4 explains in detail the fabrication steps performed for the sensor development and presents the results of the

fabricated wireless temperature sensors, low-cost impedance analyzer, and their experimental setup. Chapter 5 summarizes the thesis and briefly describes the future work.

## Chapter 2: Background and related work

A review of wireless temperature sensing results that have been reported in the literature is presented in this chapter. Presently, the state-of-the-art technologies uses complex fabrication techniques which involve the fabrication of special capacitors using temperature sensitive materials. Moreover, all of the reported techniques use inductive coupling through external inductive antenna for determining the resonance frequency, which varies with changes in electrical parameters such as inductance/capacitance. In addition, fundamental background material on electrical resonance, Y5V dielectric composition, and Y5V characterization are presented, to establish a foundation for the research.

### 2.1 Nonflexible passive wireless LC temperature sensors using LTCC (low temperature co-fired ceramics)

One of the reported techniques used interdigitated capacitor electrodes coated with thin film bismuth doped barium titanate ($Ba_{0.9}Bi_{0.066}TiO_3$) [9]. This technique demonstrated that as the temperature changes, the permittivity of the interdigitated capacitor changes; this consequently changes the resonance frequency of the sensor. The fabricated LC sensor had a fixed inductance and temperature sensitive interdigitated capacitor electrodes coated with BBT ($Ba_{0.9}Bi_{0.066}TiO_3$). This interdigitated capacitor consisted of a set of 18 electrodes of 16.72 mm in length (refer to Figure 2.1 for the sensor's cross section and dimensions). The line width of the inductor and the capacitor were designed to be 0.4 mm, the adjacent electrode spacing was designed to be 0.08 mm. The nanocrystalline BBT film of thickness of ~10mm was coated on the interdigitated capacitor.

The fabrication of this sensor involved a highly complex procedure for the preparation of the BBT powder by the controlled hydrolysis of titaniumbutoxide ($Ti(OC_4 H_9)_4$) and distilled water. The powder was then used to prepare the BBT paste and thin film. The BBT paste was prepared using the BBT powder with propylene glycol and ethanol (in known concentrations), and with distilled water. The deposition of thin film was performed manually on the capacitive part of sensor [9].
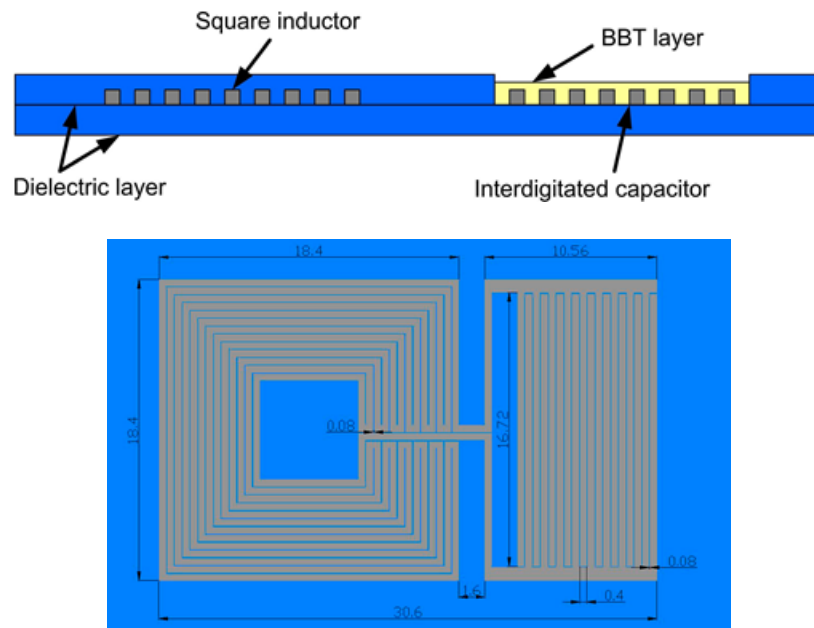


**Figure 2.1: Cross section view and dimension of the LC sensor [9].**

The fabricated sensor demonstrated a sensitivity of 62.07 KHz/°C between the temperature range of 25 °C to 165 °C. The $|S_{11}|$ parameter can be observed in Figure 2.2(a). The $|S_{11}|$ represents a ratio signal that is reflected from port 1 (output) for a signal incident on port 1 (input). Since the

capacitance value increases with an increase in temperature according to eq (1), the resonance frequency decreases. The reported observations were that the resonant frequency decreased from 571.06 MHz to 562.37 MHz as the temperature increased to 140 ℃. The fabricated sensor has many advantages such as high temperatures measurement (due to the Low Temperature Co-Fired Ceramic technology), good sensitivity, environmentally friendly (e.g., use of lead-free materials), and a linear increase in permittivity. However, a few drawbacks are the large dimensions of the device (30 mm x 10 mm), non-flexible structure, highly complex BBT powder and paste preparation process, and the manual application of the thin film coating. The manual application of the film coating can significantly affect the performance and repeatability of the sensors' fabrication, eventually, increasing the overall cost of fabrication. Moreover, the possibility of batch fabrication has also not been discussed.

$$f_r = \frac{1}{2\pi\sqrt{LC}} \tag{1}$$

where, $f_r$ is the resonance frequency, L is the inductance and C is the capacitance.
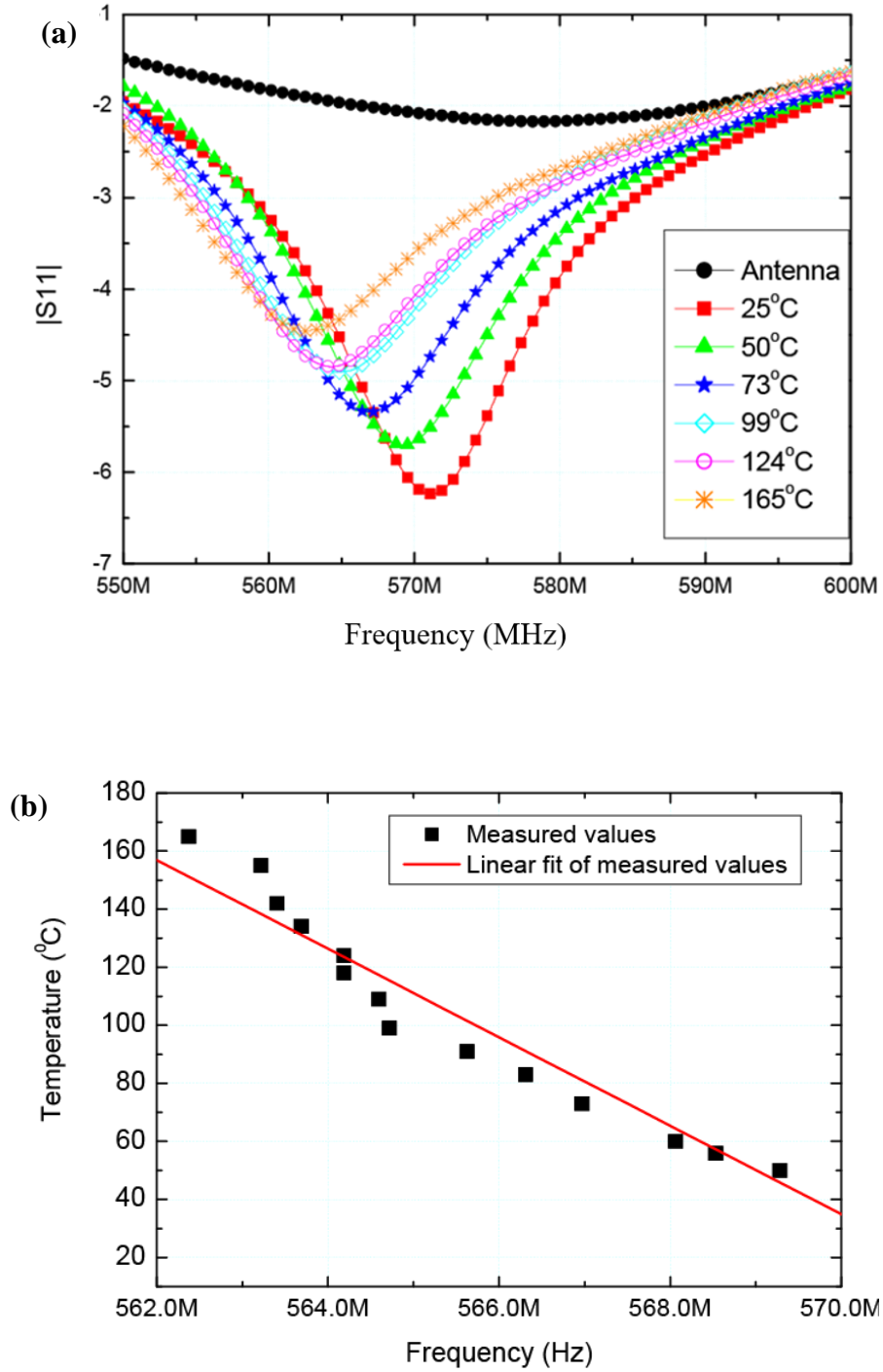
**Figure 2.2: (a) |S11 | Parameter as a function of frequency (MHz) and temperature. (b)  Temperature variation of the LC sensor w.r.t resonant frequency [9].**

A passive wireless LC sensor using a capacitive sensing approach was reported using a unique

high-K temperature sensitive ceramic material; the sensor was designed to operate in harsh

8

environments for high temperature rotating component monitoring [10]. One of the major drawbacks of using this sensor is the larger dimension of the inductor (diameter: 1.7 cm), which makes it difficult to use in compact spaces. Another wireless passive sensor that uses a Low Temperature Co-Fired Ceramic (LTCC) based on ferroelectric dielectric material was also reported [11]. This sensor demonstrated reliable results and repeatability at very high temperatures, up to 700 ℃. However, the fabrication process uses seven layers of ceramic tapes and ferroelectric ceramics are embedded in the LTCC substrate. This process makes the sensor expensive and challenging to fabricate [11].

## 2.2 Flexible wireless temperature sensors based on microparticle filled binary composite

As discussed earlier, flexible and disposable sensor have a high potential for use in diverse applications such as medical diagnostics, food safety, and environmental monitoring [12-13]. The design of a flexible temperature sensor in combination with RFID (Radio frequency identification) tags provides wireless sensors. The sensor [13] was fabricated using a nickle (Ni) micro-filled binary-polymer composite material which offered tunable temperature ranges, large resistance modulation, and improved cycling stability. The sensor test circuit consisted of a base station and a transponder as shown in Figure 2.3. The polymer composite consisted of 40 wt. % of Ni-filled particles. For the purpose of measuring the resistivity of the prepared sample, two copper foil electrodes having the dimension 5 mm x 10 mm were attached on a glass substrate with a 2 mm gap; the polymer composite was pasted within this gap having a 1 mm thickness [13].

Figure 2.4 shows the fabricated wireless sensor. The resistivity of the sample was measured using a digital multimeter, whereas the temperature was monitored using an infrared radiation (IR)

thermometer. Moreover, a flexible antenna was designed which had a 5 mm copper tape strip on a 75 μm thick PET substrate. The rectangular antenna consisted of 3 turns and area of 15 cm$^2$. The measured inductance and series resistance were measured to be 1.1μH and 0.97Ω. The base station antenna had 5 turns of copper; the diameter was 1.09 mm and it was covered with 0.45 mm thick PVC. The 5V$_{p-p}$ sine was applied to a series connection of a 4.7 nF capacitor and a loop antenna. The sensitivity of the fabricated sensor was measured to be in the range of 0.1 - 0.3V/℃ as shown in Figure 2.5. It can be observed that the resistivity of the binary composite is decreased by ~6 times by increasing the temperature by 10 ℃. The fabricated sensor has several advantages such as a flexible structure, disposable in nature, and low-cost fabrication. However, the disadvantages include larger dimensions, additional fabrication of a base station module, and a maximum inaccuracy of ±3.1 ℃, which is mainly due to the error in the alignment of the coil and the noise in the wireless circuit [13].
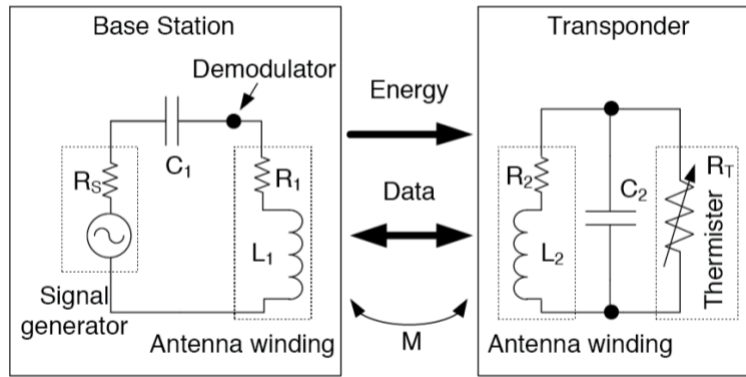


**Figure 2.3: Schematic circuit of the test sensor [11].**
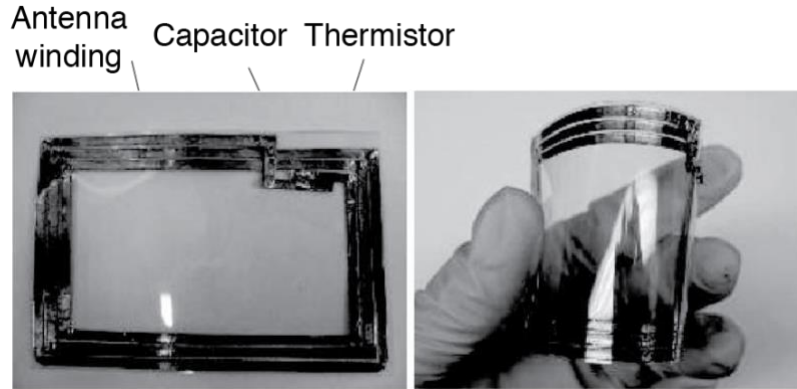
**Figure 2.4: Fabricated flexible wireless sensor [11].**
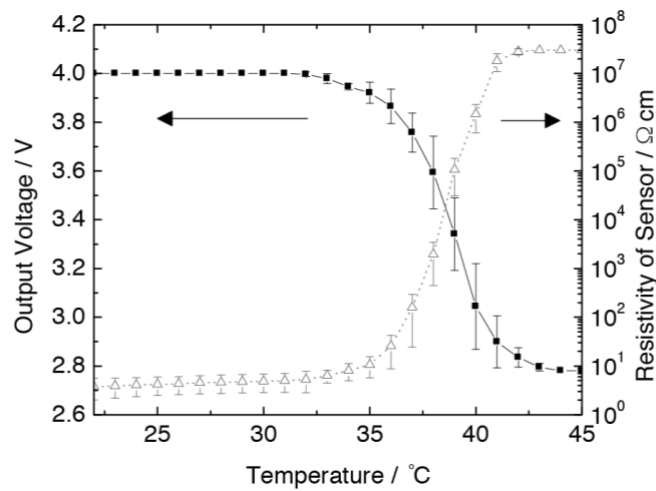


**Figure 2.5: Output voltages measured as a function of temperature [11].**

## 2.3 Open circuit wireless temperature sensors using a temperature sensitive dielectric

The wireless temperature sensing uses a temperature sensitive dielectric within an open-circuit with no electrical connections [14]. The fabricated sensor, developed by NASA, uses a novel temperature sensing technique for designing, powering, and monitoring sensors. It consists of electrically conductive material, which have electrical and magnetics fields without any electrical connections. Having this unique property, the sensor can also operate even if it's raptured or damaged which offers high reliability and longevity. The fabricated sensor inductor has the dimensions 10 cm x 10 cm, and it is prepared using a copper material. The material thickness is

10 µm; it has a spiral pattern with a line width of 2 mm and a line spacing of 0.13 mm as shown in Figure 2.6. The layer of the temperature sensitive material, whose dielectric changes as the temperature changes, is placed on either side of the spiral coil. It was observed that there is good sensitivity when the dielectric material is placed closer.
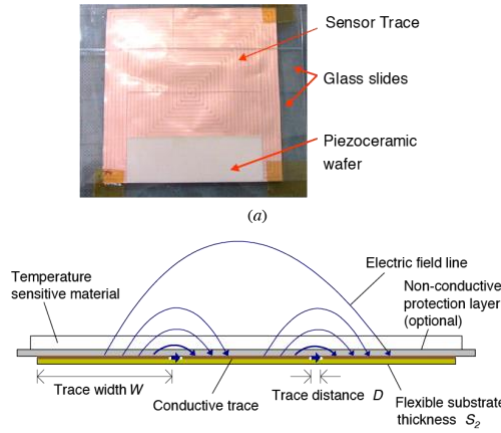


**Figure 2.6: Fabricated open circuit wireless temperature sensor [14].**

The temperature sensing was achieved by depositing a layer of the dielectric material, which is sensitive to changes in temperatures. The main advantage of having an open circuit is that a single component can provide multiple functions; this is unlike a closed circuit which consists of two components (inductor and capacitor). However, these sensor uses piezoceramics as the dielectric material which is quite complex to integrate into the fabrication process [14]. The experimental setup for the characterization of the sensor is shown in Figure 2.7. At room temperature, the measured value for the total resistance, inductance, and capacitance are 1Ω, 20.2 µH, and 3fF, respectively. The resonance frequency was measured to be 17.136 MHz. The primary dielectric materials tested were five piezoelectric ceramics TRS-100C (PZT-4, DOD Type-1), TRS-200D (PZT-5A, DOD Type-II), TRS-300HD (PZT-8, DOD Tpe- III), TRS-610HD (PZT-5A Type- IV),

and TRS-HK1HD. It was observed that the TRS-610HD ceramic had the highest sensitivity of -16.97 kHz/ ℃ for the temperature range of 21 ℃ to 160 ℃.
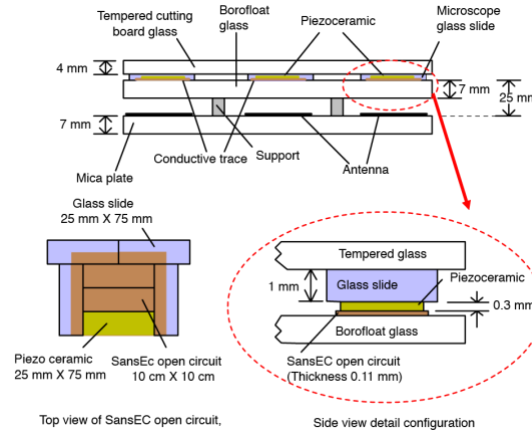


**Figure 2.7: Experimental setup of the fabricated wireless temperature sensor [14].**

## 2.4    Electrical resonance: background theory

The resonance phenomena in AC represent a unique value of frequencies which is determined by the values of the resistance, capacitance, and inductance within electrical circuit. The electrical RLC circuit are mainly categorized into two configurations: series and parallel connections. The condition for series resonance is rather simple, and it is characterized by the minimum impedance and zero phase [15-19]. The resonance phenomena occur in a series RLC circuit when the reactance of inductive and capacitive components is equal in magnitude but cancel each other due to being 180° out of phase. This produces a sharp minimum impedance which is very useful in tuning applications. This sharpness of a minimum impedance depends on the value of the resistance (R). A lower value of resistance gives a sharper minimum impedance, and conversely for higher values of R. The Figure 2.8 shows the schematic of series and parallel RLC circuits. The resonance in a parallel RLC is more complex. It is defined as the frequency at which the

13

parallel impedance is the maximum, or the frequency at which the current is in phase with the voltage producing unity power factor [15-19].

**(a)**                                                     **(b)**
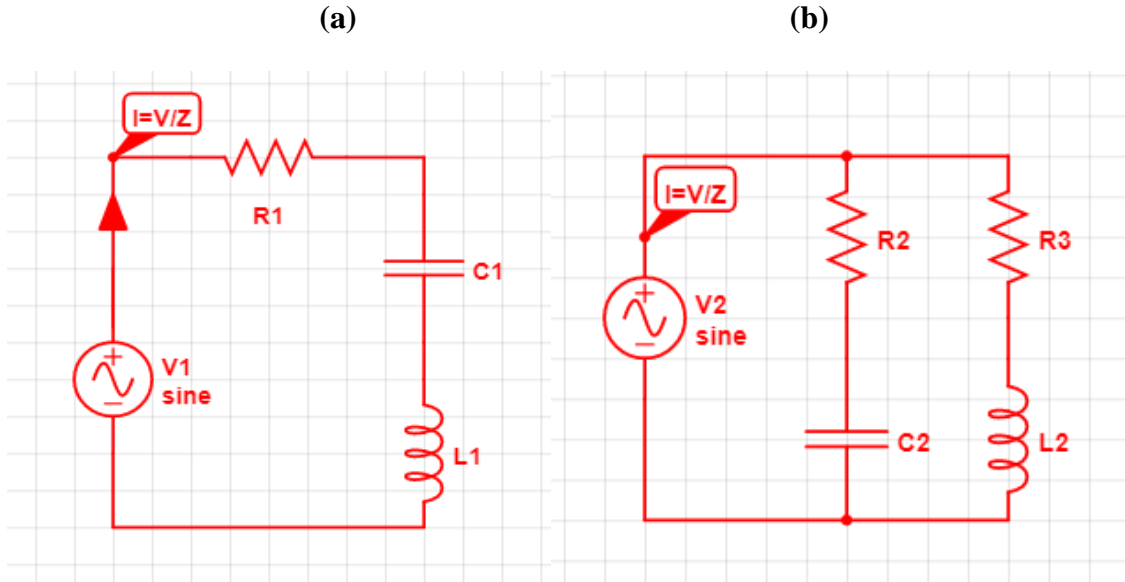


**Figure 2.8: Schematic of RLC resonance circuits (a) RLC resonance circuit in series and (b) RLC resonance circuit in parallel.**

## 2.5   Y5V dielectric composition

The Y5V dielectric composition was first invented by James M. Wilson, Thallam T. Srinivasan and Victor, N.Y. [20] and was patented on Feb 18th, 1997 under Ferro Corporation, Cleveland, Ohio.

The Y5V dielectric had a composition of barium titanate host material $((Ba_xCa_y), (Ti_zSn_w)O_3)$, where x,y,z, and w are the molar ratios of barium, calcium, titanium, and tin, respectively; the material also had a small amount of PbO (~0-2.0 wt. %). This material was then doped with small amounts of a lead boro alumino silicate frit, and one or more of the following: boric acid, the oxides of La, Zn, Cu, Nb, Mn, and Y. The result was a dielectric ceramic composition suitable for

14

making low fired multilayer capacitors exhibiting Y5V characteristics; the composition had high dielectric constants in the range of 11000-14000.

The barium titanate based material was prepared by using barium (Ba), calcium (Ca), titatium (Ti), and tin (Sn) compounds which had a small amount of lead oxide (PbO). The mole fraction of Ba, Ca, Ti, and Sn were represented by x, y, z, and w, respectively. The value of "x" was ~0.90-0.92 in x+y, and the value of z was ~0.86-0.89 in z+w ; these elements were added to the lead oxide in the amount of t wt. % PbO. The host materials $(Ba_xCa_y)$ and $(Ti_zSn_w)O_3$ had molar ratios of (x+y) to (z+w) greater than one. Furthermore, x+y equaled ~1.03 moles; z+w equaled 1 mole, and t greater than ~0-2 wt. %. Having the same ionic size of Ba and Pb, it is believed that Pb may enter the perovskite structure by removing Ca ions. These removed Ca ions may occupy interstitial sites. The above host material was then calcined at 1050 ℃ for two to six hours. The calcined material was turned into powder and then doped with small amounts of: lanthanum (0.1 to 0.5 wt.%); and/or zinc (0.4 to 1 wt.%); and/or copper (0.1 to 1.0 wt.%); and/or niobium (0.1 to 0.8 wt.%); and/or manganese (0.1 to 1.0 wt.%); and/or yttrium (0 to 0.3 wt.%); and/or boric acid (0 to 1.25 wt.%), in addition to a glass frit (lead boro alumino silicate). The mixture was fluxed, dried, and subjected to a size reduction process in a conventional manner. The above sample composition was then used to make multilayer capacitors using a standard tape casting and building technique. These multilayer ceramic capacitors (MLCCs) were then fired at 1130 ℃ for five hours in a box type Klim. It was observed that if the quantity of glass frit was reduced slightly, the value of the dielectric constant tended to increase in the range of 15000 to 16000. The standard tape casting and building technique is shown in Figure 2.9. The sample composition for one Y5V capacitor undergoes a similar manufacturing process for the mass production of Y5V capacitors [20].

15
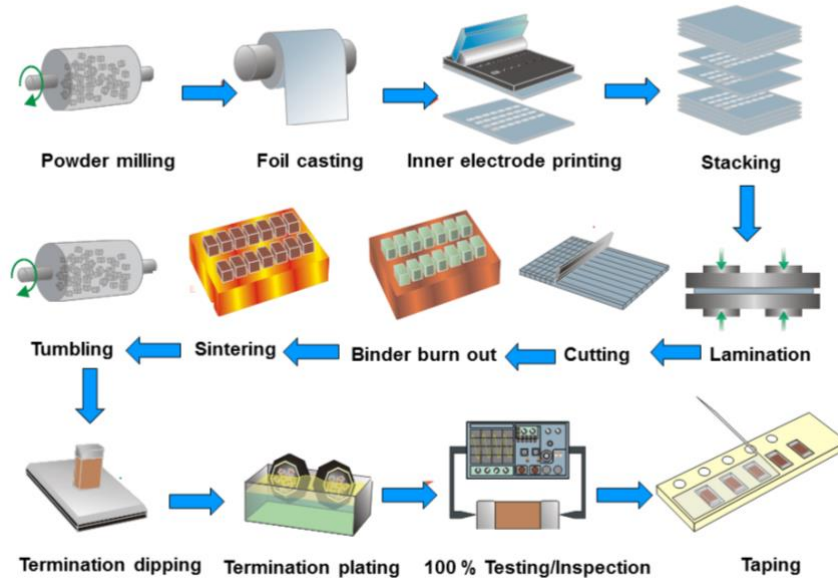
**Figure 2.9: Industry standard manufacturing process for MLCC capactors.**

As the Y5V capacitors exhibit a strong dependency on the change in capacitance with a rise in temperature, this capacitor is selected for varying the resonant frequency of the LC-tank sensor in the proposed flexible wireless temperature sensor design (refer to Chapter 3).

## 2.6 Characterization of Y5V capacitors

MLCCs are mainly available in two major classes: Class 1 and Class 2 formulations. Class 1 represents temperature compensation formulation, whereas Class 2 represents stable temperature and general applications formulation. Class 2 capacitors are typically based on the chemistry involving mainly barium titrate and provides wide range of capacitance value and temperature stability. The commonly used Class 2 dielectric is X7R which provides intermediate capacitance values having only ±15% change in capacitance over an operating range of -55 ℃ to 125 ℃. It's mainly applicable where a high stability in capacitance value is required over wide temperature

16

ranges. However, the Y5V capacitor provides a high capacitance value and is suitable for applications where a strong temperature dependency is expected. The Y5V capacitance value can vary from +22% to -82% over -30 ℃ to +85 ℃. Various types of Y5V multilayer dielectric capacitors are commercially available in the form of low-cost ($0.01-0.10) surface mount chips. Their strong temperature dependency and low-cost may allow them to serve as the sensing element in an LC tank circuit for frequency based wireless temperature reading. The Y5V capacitor are commercially available for 4.7 µF, 10 nF, and 1000 pF from Murata, Vishay, and AVX. Here, capacitors from Murata Electronics are studied and characterized for three different frequencies of 10 KHz, 100 KHz, and 1 MHz (refer to Chapter 3).

# Chapter 3: Novel LC passive wireless temperature sensor: design, fabrication, and characterization

## 3.1    Experimental setup

The characterization of various Y5V capacitors was performed using a hot plate and an HP LCR meter. The surface mounted device (SMD) MLCC from Murata Electronics (part #: GRM216F51E102ZA01D) capacitor was mounted on the glass slide using copper tape. The two thin insulted wires were connected at both ends of the capacitor; the change in the capacitance was monitored using the LCR meter. The temperature on the capacitor was checked using the thermocouple and the IR gun before proceeding with the measurements. Based on this check, it was determined that the temperature of the hot plate required a ~10 ℃ compensation due to the glass slide. Therefore, in order to achieve the temperature of 30 ℃ on surface of the capacitor, the hot plate temperature was set to 40 ℃. During the experiment, a wait time of 10 mins was provided after each reading to acquire stable readings throughout the experiments. In this research we studied the effect of varying the input frequency over 10 KHz, 100 KHz, and 1 MHz. The HP LCR meter provided the capability to change the input frequency from 1 KHz to 1 MHz.

## 3.2    Measurement results

The characterization of the 4.7 µF, 10 nF, and 1000 pF Y5V capacitors was performed using experimental setup (Section 3.1) with the input frequencies of 10 KHz, 100 KHz, and 1 MHz. Figure 3.1(a) shows the linear relationship of the drop-in capacitance with the applied temperature at the 10 KHz frequency. All of the Y5V capacitors were then compared with the commercially

available 100 pF NPO MLCC SMD (part no: GRM21A5C2J101JWA1D) capacitor from Murata Electronics. The capacitors were heated from 27 ℃ (room temperature) up to 75 ℃ using the hot plate. As the temperatures increased, all three components presented a decreased capacitance. The 4.7 μF capacitor demonstrated the highest drop in the capacitance, which was 66.65% at the maximum temperature of 75 ℃. The 10 nF capacitor dropped nearly 50% at 75 ℃. The most modest drop in the capacitance was ~12% for the 1000 pF capacitor at the same temperature. The 1000 pF capacitor only showed a ~4% drop in capacitance between 27 ℃ to 45 ℃. Moreover, no change in the capacitance value was observed for the commercially available NPO series 100 pF capacitor.
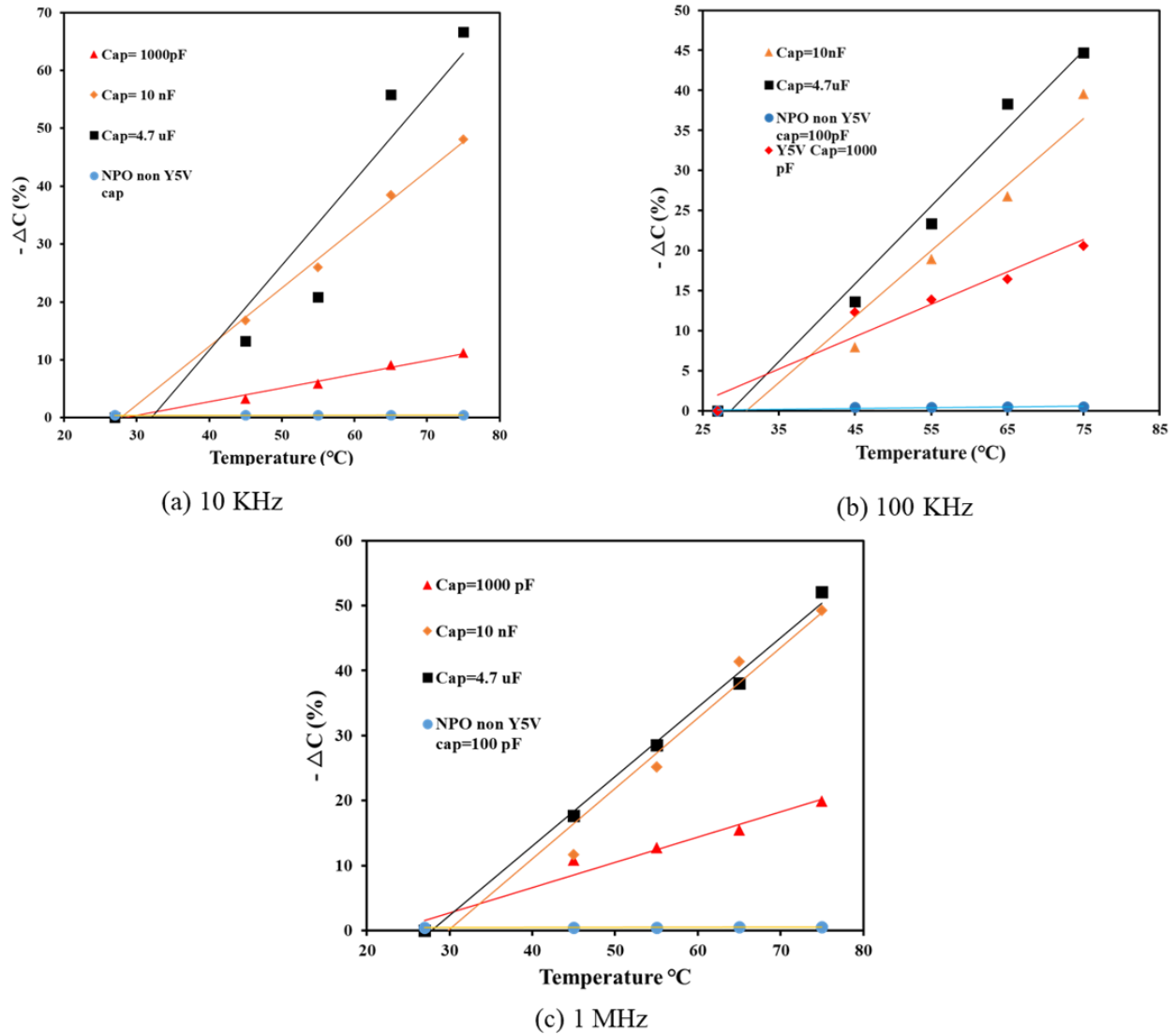
**Figure 3.1 : Characterization results of Y5V capacitors at (a) 10 KHz frequency, (b) 100 KHz, and (c) 1 MHz.**

Using the same experimental setup and Y5V capacitors discussed in the previous section, the input frequency was changed to 100 KHz. Figure 3.1(b) shows the linear relationship between the drop in capacitance and the applied temperature at the 100 KHz frequency. The input frequency of 100 KHz was applied using the HP LCR meter. The highest capacitance drop of 52.12% was observed for the 4.7 µF capacitor at 75 ℃; the capacitance dropped to approximately 2.25 µF. The 10 nF

capacitor demonstrated a capacitance drop of ~50% at 75 °C whereas, the 1000 pF capacitor showed a drop-in capacitance of ~11% at 45 °C and ~20% at 75 °C

The characterization of the Y5V capacitors was again performed using same setup, but with the input frequency of 1 MHz provided by the HP LCR meter. As shown in  Figure 3.1 (c), it was observed that the 4.7 µF capacitor capacitance dropped to 2.6 uF at 75 °C, which is a ~45% change in the capacitance. A similar trend was also observed for the 10 nF capacitor; it exhibited a ~40% of drop in capacitance at 75 °C. A ~13% drop in capacitance was observed at 45 °C and a 21% drop at 75 °C for the 1000 pF Y5V capacitor.

Three Y5V Capacitors having values 4.7µF, 10 nF, and 1nF were characterized using the experimental setup discussed in Section 3.1 at three different frequencies (10 KHz, 100 KHz, and 1 MHz). With respect to sensitivity, it was observed that the 4.7 µF at the 10 KHz input frequency demonstrated the highest sensitivity of 65 nF/ °C, the 10 nF showed the highest sensitivity of 102 pF/ °C at the 100 KHz input frequency, and the 1 nF capacitor illustrated the highest sensitivity of ~5 pF/ °C at the 1 MHz input frequency. Although the 4.7 µF capacitor proves to have highest sensitivity, the 1 nF capacitor with a resonance frequency below 20 MHz was selected for the final design. This decision was based on two main reasons. Firstly, it satisfies the research goal of miniaturizing the sensor size (~ 5 mm). The commercial SMD 4.7 µF capacitor is available in the smallest footprint of 3.20 mm x 2.5 mm and thickness of 0.5 mm which quite large as compared to 1000 pF capacitor size. Secondly, the 1000 pF capacitor offers acceptable sensitivity in the desired resonance frequency of 1 MHz and offers a better Q-factor for the LC circuit than either

the 4.7 µF or 10 nF capacitors. Therefore, from equation (2), a lower the capacitance value results in a higher Q-factor in a Series RLC circuit. The Q-factor is given by eq (2) below:

$$Q = \frac{1}{R}\sqrt{\frac{L}{C}} \qquad (2)$$

Where, R is series resistance, L is inductance, and C is capacitance.

## 3.3 Development of the discrete LC circuit using a 1000 pF capacitor

To establish the proof of concept before the actual fabrication of the planar sensor, a discrete LC tank circuit was prepared using a 1000 pF Y5V capacitor and a hand wound inductor. The properties of the fixed inductor are shown in Table 3.1:

Table 3.1:Properties of the inductor wire used in the discrete LC coil

| Parameter | Value |
|---|---|
| Wire Diameter | 0.64 mm |
| Inner Diameter (loop) | 37.75 mm |
| Resonant Frequency | 1.75 MHz |
| DC resistance | 0.4 Ω |
| Number of Turns | 15 |
| Inductance | 10.44 µH |

The inductance of the coil was measured to be 10.44 µH using an HP 4275A Multi-frequency LCR meter at the input frequency of 1 MHz. The inductor was prepared by tightly winding the conducting wire without overlapping turns; the wire properties are summarized in Table 3.1 The turns were fixed in place by applying the hot thermal glue gun all over the surface of the inductor.

22

The 1000 pF capacitor was first pasted on the glass slide with two copper tape (pads) separated by a distance of 0.3 mm. Thin insulated copper wires were soldered at both terminals along with the hand wound inductor. The prepared sample is shown in Figure 3.2. The resonance frequency was observed to be 1.75 MHz.
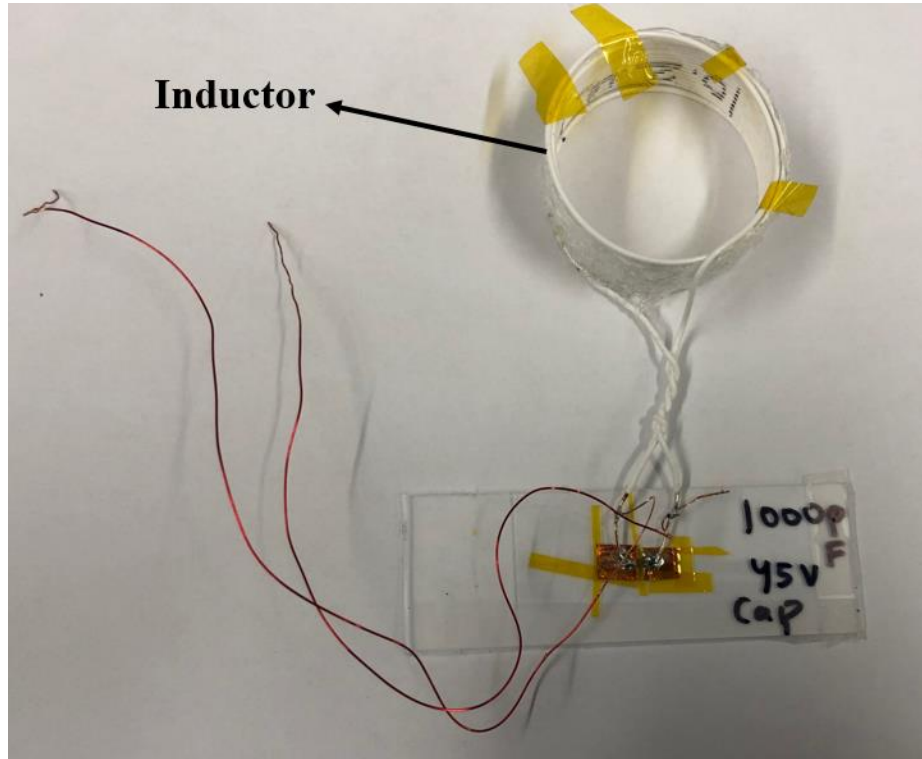


**Figure 3.2: Discrete LC resonant sample with a 1000 pF Y5V capacitor.**

The equivalent schematic circuit is shown in Figure 3.3(a) where the sensor is represented by the load coil and the external antenna, connected with the Agilent device, is shown on the other side.

### 3.3.1 Experimental setup

The experimental setup is shown in Figure 3.3(b). The LC discrete sample was firmly attached onto the Fisher Scientific Hot Plate (CAT no. SP88857290 V ~ 100-120 AMPS: 13 Hz 50/60) and

the temperature was set to 27 ℃ for the initial measurement. A single loop external antenna was used; it was connected with the Agilent 4396B spectrum-impedance analyzer. The diameter of the external antenna used was the same as the diameter of inductor prepared for the LC discrete circuit. This achieved good coupling between the coils. The separation distance between two coils was set at ~ 2 mm for the best results. The measurements were made by increasing the temperature of the hot plate from 27 ℃ to 75 ℃. The wait time between two consecutive measurements was 10 mins, which allowed the temperature to stabilize before the taking the next measurement. The Agilent analyzer was well calibrated (Open and Short circuit) using the calibration kit provided by the manufacturer before making any measurements.
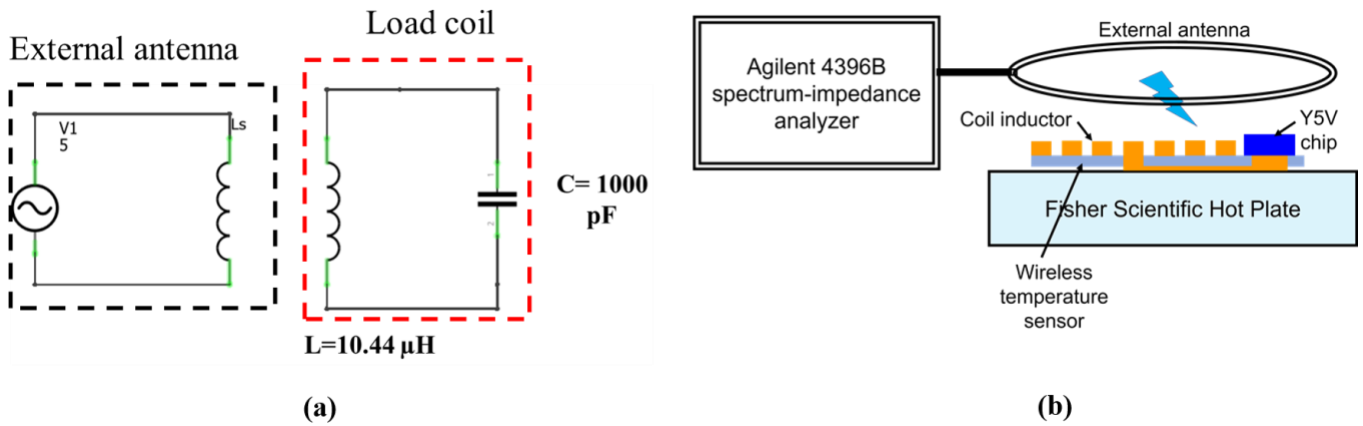


**Figure 3.3: (a) Equivalent schematic representation of a larger sensor device (b) Experimental setup for characterizing the discrete LC resonant circuit**

### 3.3.2 Measurement results

By using the experimental setup as discussed in Section 3.3.1, the shift in resonance frequency was recorded using the Agilent 4396B spectrum-impedance analyzer for a frequency sweep from 1 MHz to 2.5 MHz. The results are illustrated in Figure 3.4. For example, the resonance frequency

observed at 27 ℃ was 1.75 MHz. Approximately, an 800 KHz resonant frequency shift was observed over the temperature increase of 48 ℃, and a resulting sensitivity of 16.66 KHz/°C. The recorded frequency response of the LC discrete circuit on Agilent is shown in Figure 3.4, and its trend with temperature change is displayed in Figure **3.5**. For comparison with the measured resonant frequencies, Figure **3.5** also includes resonant frequencies (denoted as "theoretical data") that were calculated using the capacitance changes measured with varying temperatures (for the 1000 pF capacitor, as discussed in Section 3.2) and a measured constant inductance value of 10.44 µH using eq. (1). The resonant frequency ($f_r$) values observed have relatively good agreement with the measured value. The error between the measured and theoretical values is calculated to be ~6.4% initially and progressively decreases to ~3.2% with higher temperature measurements.
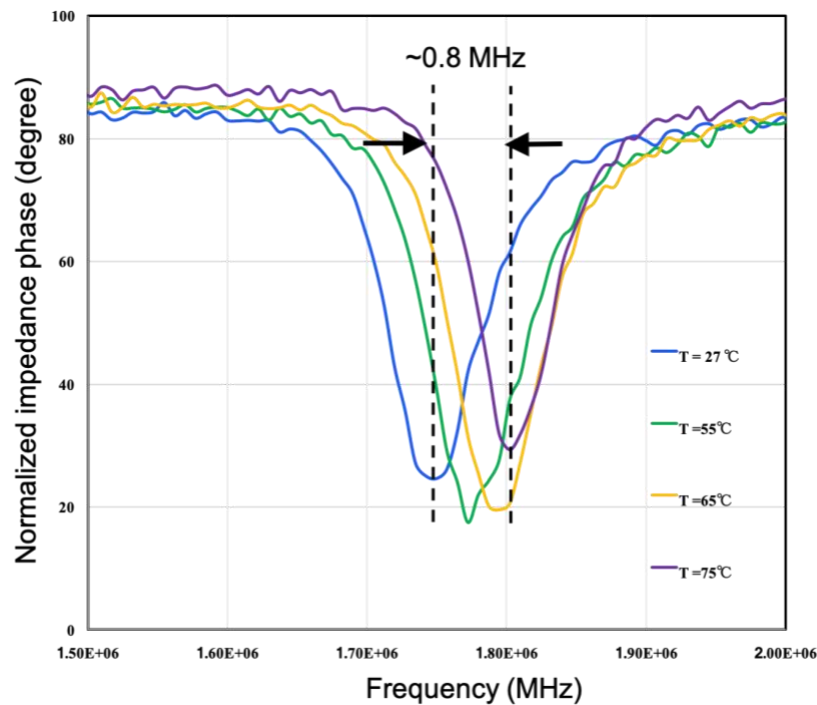


**Figure 3.4: Measured temperature response of the resonant frequency of the LC discrete device**

25
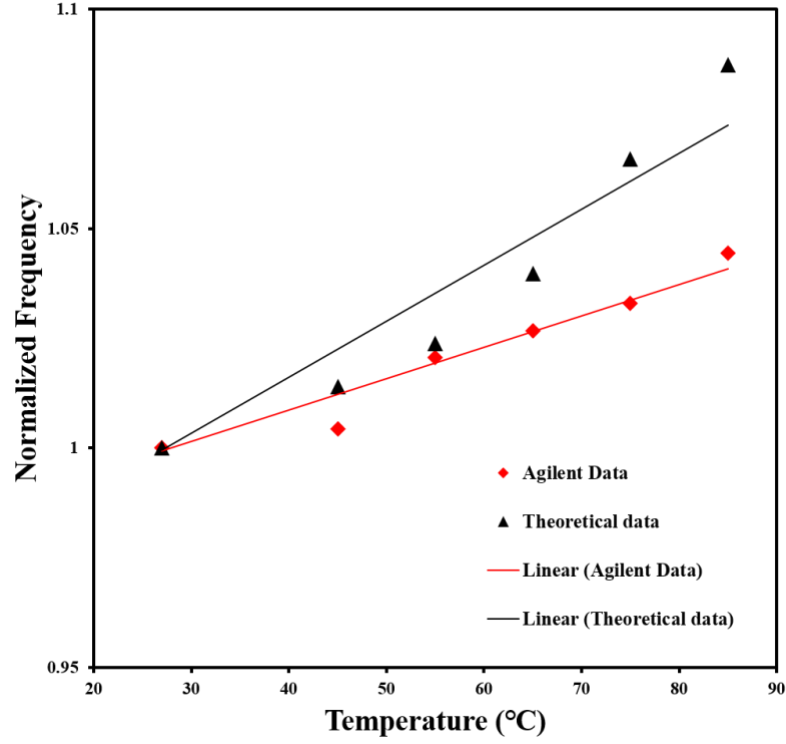
**Figure 3.5: Comparison of the measured and calculated value changes of ($f_r$) with temperature.**

### 3.3.3    Summary

The discrete LC circuit having a fixed inductance of 10.44 µH and a 1000 pF Y5V capacitor was fabricated and characterized. The Agilent Impedance analyzer and Fisher Scientific Hot Plate were used for monitoring the shift in the resonance frequency and the heating device, respectively. The fabricated discrete LC resonant circuit demonstrated a sensitivity of 16.66 KHz/ ℃ for a 48 ℃ increase in temperature. Therefore, from this experiment it can be concluded that the proposed device concept proves to be working with acceptable sensitivity and motivates the work towards the fabrication of the planar coil devices.

### 3.4    Design and fabrication of the planar resonant coil

As discussed in previously, printed flex-circuit sensor circuits have a number of advantages including smaller size and simplicity of fabrication. An extensive body of research has been reported on modelling and designing planar LC coils [21-24]. The main objective of this section is presenting the design of the fixed inductor which allows the mounting, or integration, of the commercial Y5V capacitor sensing element to form an LC resonant circuit. The passive resonant circuits are formed by the planar inductor ($L$) and the parallel plate capacitor (C) as shown in Figure 3.6.
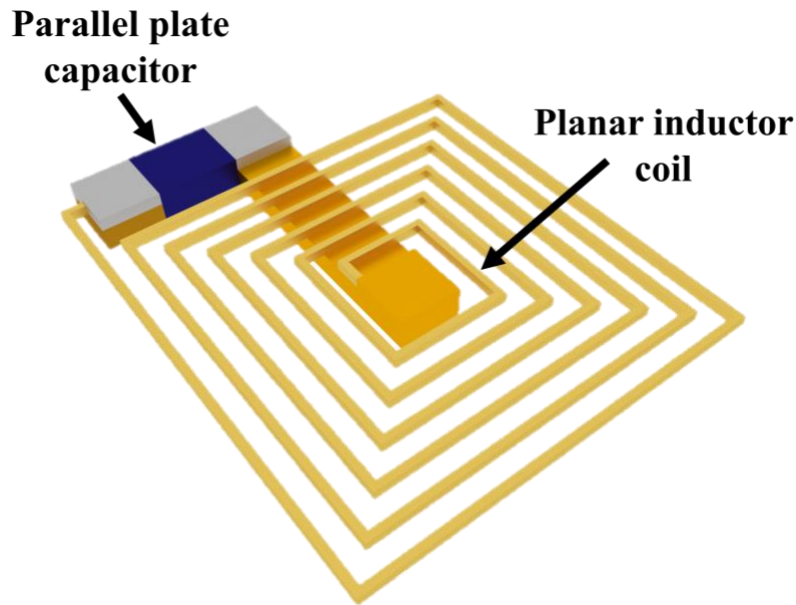


**Figure 3.6: Illustrative 3-D model of the proposed LC resonator**

Significant research has been done for accurate modelling of planar inductor coils using lumped circuit models [15] [24-30]. The model presented by Wheeler model was simple and accurate [26]. Based on the Wheeler model, the square planar coil used for inductance calculations can be estimated by using eq (3) below:

$$L = \frac{k_1 u_0 n^2 d_{av}}{1+k_2 e_{ff}} \tag{3}$$

where, $k_1 = 2.34$ and $k_2 = 2.75$ are coil shape dependent co-efficient, $n$ is number of turns, $\mu_0$ is permeability of free space, $d_{av}$ and $e_{ff}$ are fill ratios given as in eq (4) below [26]:

$$d_{av} = \frac{dOUT + din}{2} \quad \text{and} \quad e_{ff} = \frac{dout - din}{dout + din} \tag{4}$$
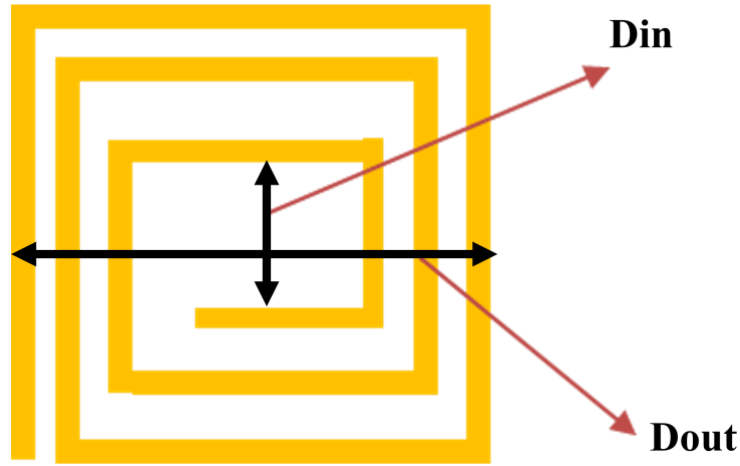


**Figure 3.7: Illustrative representation of Square type planar coil (turns = 3).**

The commercial parallel plate Y5V capacitor was used as the temperature sensing device in the circuit. Therefore, using the above model, estimates for of the inductance values can be calculated and the planar circuit having the desired resonant frequency can be fabricated. The wireless temperature sensor was fabricated on Cu-clad PI (Polyimide) substrate from Dupont which offers an economic and simple implementation. Moreover, PI has bio-compatibility properties and is widely used in the fabrication of implantable devices. Furthermore, the use of Cu-clad PI also

28

offers a base platform for flexible-circuit technology which is well established for electronics circuit fabrication [31-36].

## 3.5 **Fabrication of large size wireless temperature sensor**

In this section, the fabrication of the passive wireless temperature sensor circuit in two different sizes (25 mm$^2$ and 6 mm$^2$) is discussed. The larger coil (25 mm$^2$) was primarily designed as preliminary prototype for testing the proof of concept. Therefore, to establish the proof of concept it was decided to first develop the larger device ($\sim$ 25 mm$^2$). The fabricated L coil was mounted with the Y5V 10 nF SMD capacitor chip (Series 1206 Yageo dimensions 3.2 x1.6 x 0.25 mm$^3$) to complete the LC loop. The surface mounting of the capacitor was performed manually under a microscope using CW2400 conductive epoxy and curing it for 45 mins at 100 ℃ on the hot plate. The fabricated wireless temperature coil is characterized and validated using theoretical measurements. The both sensors were fabricated using the same fabrication technology; however, different materials and a different mask design were used to achieve better results for the miniaturized sensor design of 6 mm$^2$.

### 3.5.1 **Mask design**

The 20 mm wireless temperature sensor mask was designed with the dimensions presented  Table 3.2. The theoretical value of the inductance was calculated to be 1.3 µH using eq (3) and (4).

Table 3.2 Parameters for the larger inductor coil

| Parameter | Dimensions |
|---|---|
| Number of Turns | 10 |
| $D_{in}$ (mm) | 4 |
| $D_{out}$ (mm) | 22 |
| Line Width ($L_w$) ($\mu$m) | 500 |
| Line Spacing ($L_s$) ($\mu$m) | 500 |
| Coil Dimension (mm$^2$) | 22 x 22 |

The complete design consisted of three masks: two dark field masks having features connecting the electrode design and the inductor coil pattern, respectively; and one clear field mask having contact two Vias/holes of dimensions 200 $\mu$m each. The conceptual mask design is illustrated in Figure 3.8.
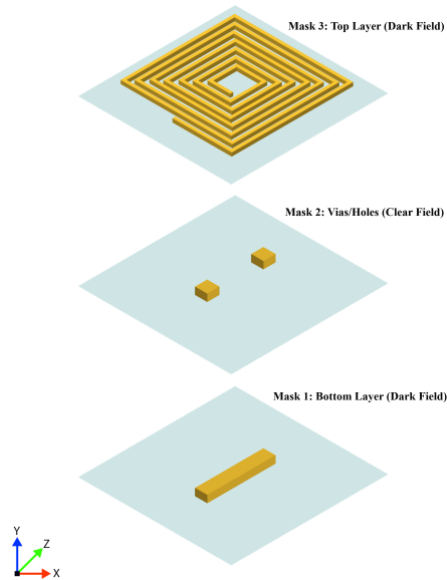


Figure 3.8: Illustrative model of the mask design of the inductor coil

30

### 3.5.2  Fabrication process

The first prototype of the wireless sensor was fabricated as illustrated in Figure 3.9. The previous studies indicate using single sided Cu-clad PI [27] [32]. However, our fabrication technique utilized a novel approach using Double-sided Cu-Clad PI, which offers fewer cleanroom fabrication steps and faster prototyping than conventional technology. A double-sided Cu-clad PI (Pyralux AP8515R Dupont Co. USA) with a 25-µm thick PI and an 18-µm thick Cu on both sides is used in this effort. The photolithography for circuit fabrication is performed with Dry Film photoresist of 19 µm thickness (MacDermid SF 306). The complete overview of the fabrication process is shown in Figure 3.9 (a) - (m).

Firstly, the 18 µm double sided Cu-clad from Dupont pyralux (AP8515R) with the exact size of the mask was cleaned using RONA clean and rinsed with DI water as shown Figure 3.9(a). Secondly, as shown in (b) a negative PR of 19 µm was laminated over the Cu substrate on both sides. The sample was then flipped as shown in (c) and mask 3 was placed (contact path) in close contact with the substrate and exposed in UV light for 9 seconds. Three rounds of the PR development process were performed as shown in (d), which used a mixture of $Na2CO_3$ (Sodium Bicarbonate) and DI water. Thirdly, the copper etching process as shown in (e) was performed for creating the Vias between the top and bottom layer; this used 200 ml of the Cu etching solution. The sample was agitated continuously during the process. Again, as shown in (f) the sample was laminated on the bottom layer with the PR (19 µm) and UV exposure was performed from the bottom of the substrate as shown in (g). Mask 2 (Vias) was kept in close contact with substrate and the sample was exposed in UV light for 9 seconds.

Moreover, as shown in (h) to expose the bottom layer Cu layer, PI etching was performed using the PI etching solution (a mixture of KOH, Ethanolamine, and DI water). The total time for etching the 250 µm Vias was observed to be a maximum of 9 mins; the temperature was stable at 87 ℃ of the PI etchant solution. For establishing a good electrical connection between the top and bottom Cu layers, electroplating was performed. To achieve this task the Vias were filled with copper material as shown in (i). Parameters were set at a starting Voltage of 0.2 V and a current of 0.09 amps. It was observed that the current gradually increased as time passed and the process was stopped when current no longer increased.

Lastly, the inductor coil was patterned on the top layer of the sample. The PR laminating and development, UV exposure and copper etching, and PR stripping was performed for patterning the inductor coil on the top side as shown in (j), (k) and (l), respectively. The fabricated coil was then dried using an air gun. Lastly, as shown in (m) the 10 nF Y5V commercial capacitor was bonded on the two terminals of the inductor manually using Chemtronics CW2400 conductive epoxy and allowed to cure on the hot plate for 1 hour at 100 ℃.
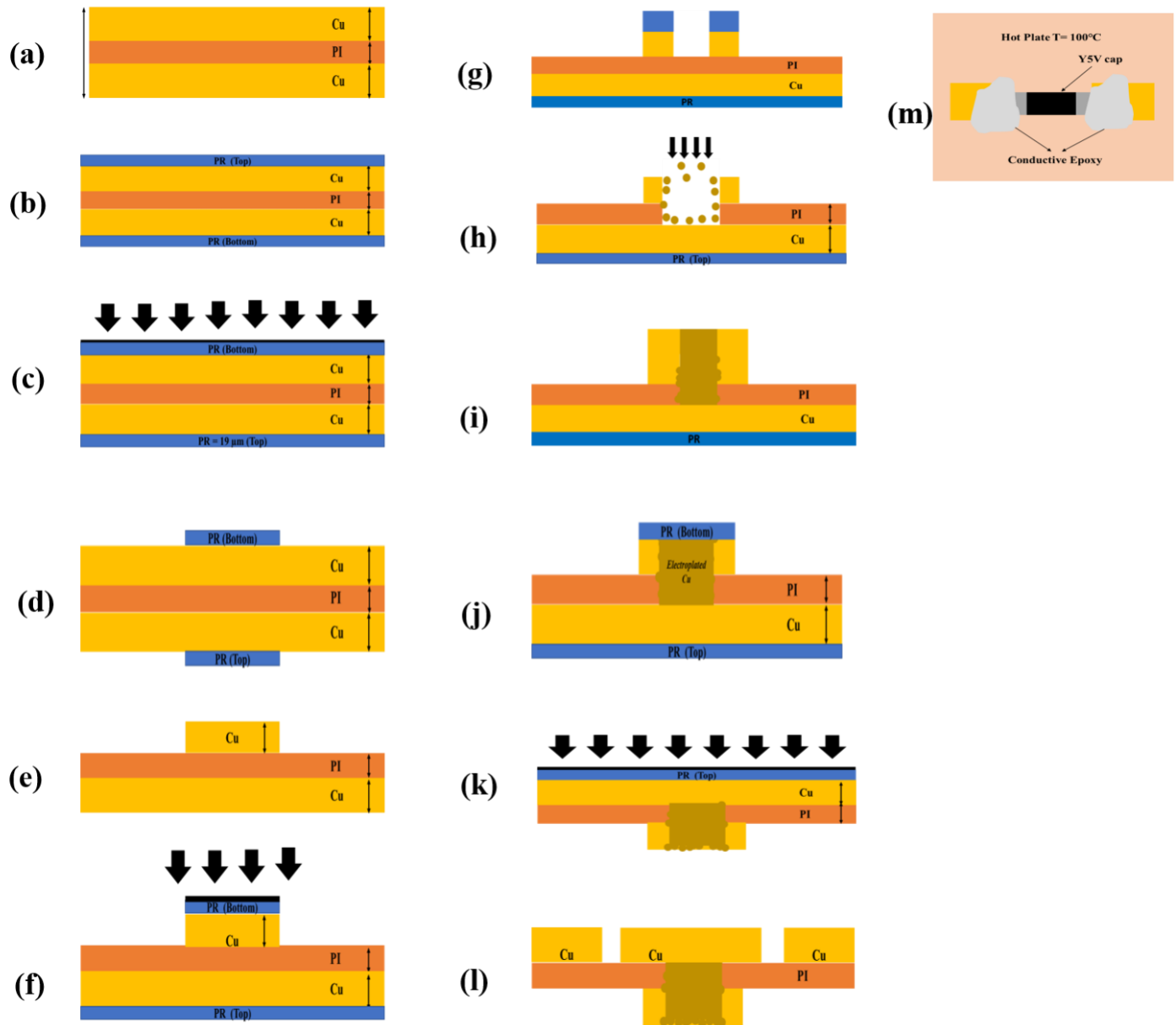
**Figure 3.9: Fabrication process overview for the inductor coil**

### 3.5.3    Characterization results

The fabricated inductor coil was characterized using setup shown in Figure 3.3(b). The fabricated Inductor coil along with the 10 nF capacitor formed the LC resonant circuit, as shown in Figure 3.10. The inductance of the larger LC coil was measured to be 1.55 µH which is close to the theoretically calculated value of 1.3 µH; the Q-factor was measured to be 28. The resonance frequency tracking was performed using the Agilent 4396B spectrum impedance analyzer through an external antenna coupled with the device as shown in Figure 3.11. This device was subjected to changes in temperature from 27 ℃ to 70 ℃ by using the Fisher scientific hot plate. The device demonstrated a good resonance dip of 155.34 MHz revealing a frequency response of 106-150 KHz/ ℃ as shown in Figure 3.12. The total resonance frequency shift of ~5.1 MHz was observed for the temperature rise of 43 ℃. Figure 3.13 depicts the comparison of the resonant frequency shift between the measured value and the theoretical (calculated) value, with respect to the rise in temperature. The theoretical values (plot shown in Figure 3.13) were determined using eq. (1) by measuring the inductance of fabricated large size coil and the capacitance of the particular chip at different temperatures varied on the hot plate, both at the resonance frequency of device (~155 MHz).

Due to the relatively higher resonance frequency (compared to those of the discrete LC sensor and the miniaturized sensor to be discussed later), these inductance and capacitance measurements used spectrum/impedance analyzers (Agilent 4396B and E5061B, respectively).    These measurements showed that both the inductance and capacitance were substantially lower (approximately 23 nH and 60-80 pF (depending on temperature), respectively) than their DC/low-frequency values at the particular frequency. The error between the measured and theoretical

values is calculated to be ~18.3% on average, with a decreasing trend with temperature similar to the discrete device case. The level of error is relatively large compared with the cases of the other two device. A possible reason behind this might be that the coil's inductance largely depended on the relatively high operating frequency and this was measured using the impedance analyzer through wiring to the coil which might have affected the measured values of the inductance.
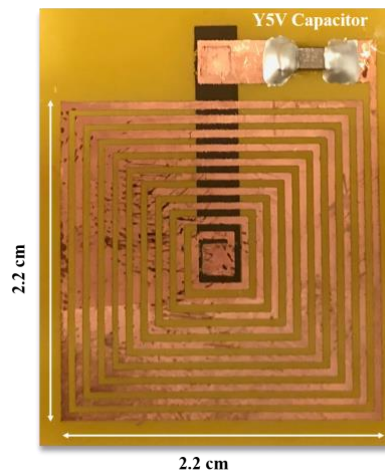


**Figure 3.10: Larger (~ 20 mm$^2$) LC resonant fabricated coil area dimensions**
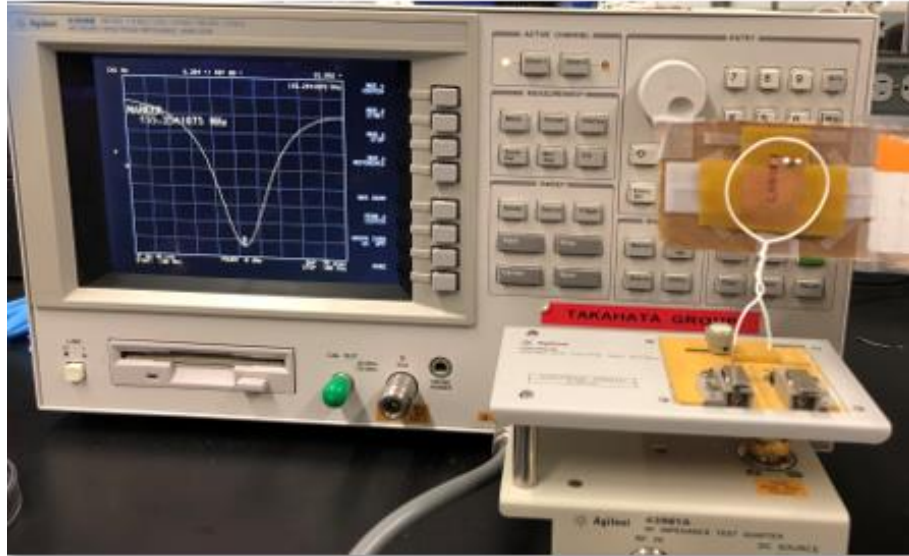
**Figure 3.11: Resonant frequency measurement on the Agilent spectrum analyzer experimental setup with an external antenna**
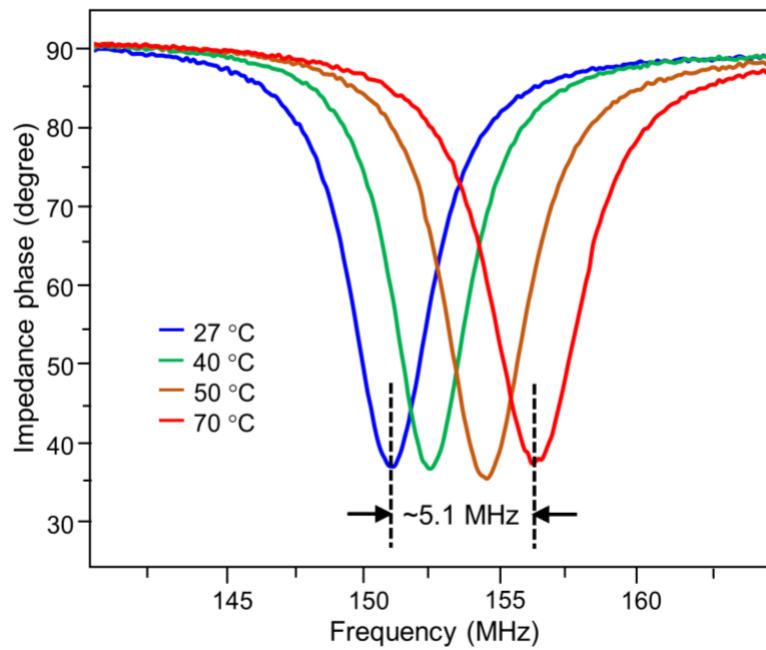


**Figure 3.12: Preliminary test results using a larger-area (20-mm$^2$) device: measured phase dip shifting with respect to temperature.**
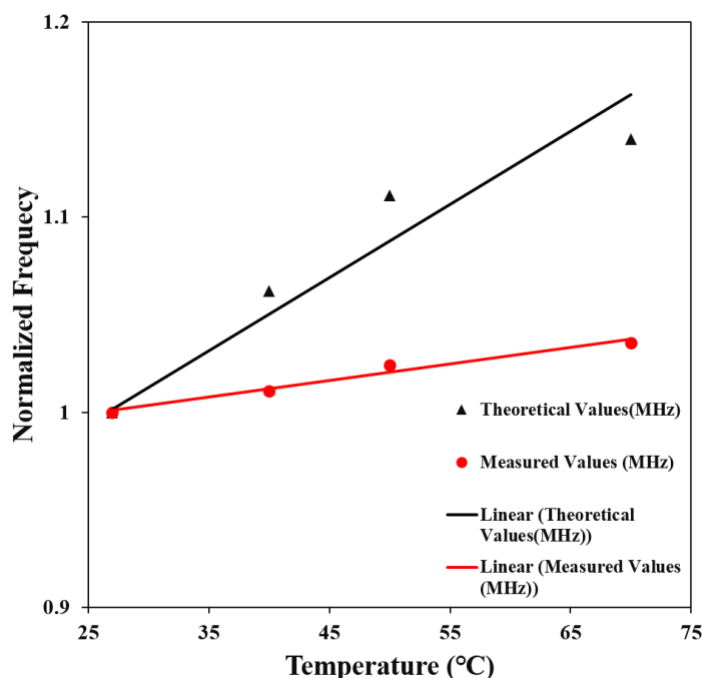
**Figure 3.13:Comparison of the shift in the resonant frequency w.r.t temperature in the ~20 mm$^2$ coil: measured value (red) vs. theoretical value (black).**

### 3.5.4    Flow loop testing experiment

The wireless temperature sensor can prove to be very useful in critical chemical processes where the continuous temperature monitoring of fluid flow is essential, especially in hazardous environments. Such wireless sensors can be located on the surface of the tubing/piping containing fluid and the temperature of the fluid can be easily monitored. Monitoring temperatures is very important, and wireless temperature sensors can be very useful tools for safety management in such processes.

To better demonstrate the potential application of this sensor, an experiment was performed using a Cole-Parmer polystat temperature-controlled circulating bath. The illustrative and experimental

setup are shown in Figure 3.14 and Figure 3.15, respectively. The capacitor chip was located on surface of the tubing connected with the help of the tubing attachments of the temperature-controlled circulating bath, and the resonance frequency shift was monitored using the Agilent impedance analyzer.
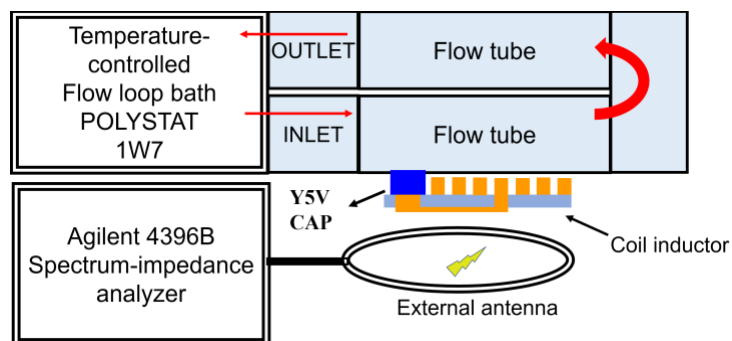


**Figure 3.14 Flow-loop experimental setup**
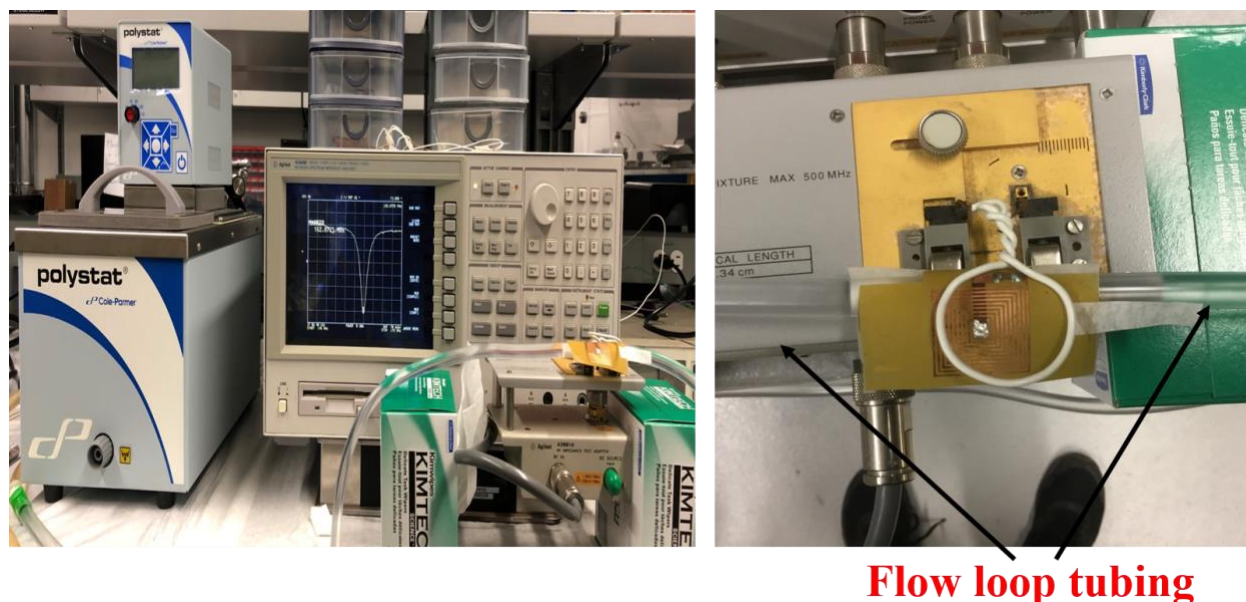


**Figure 3.15: Experimental setup of the flow loop testing using the larger sensor.**

The DI water was used as the process fluid for this experiment. The heating circulation bath temperature was controlled by the user. The measurements were performed at five different temperatures: 25 ℃, 45 ℃, 55 ℃, 65 ℃ and 75 ℃. The external antenna connected on Agilent device was used for wirelessly monitoring the resonance frequency at each temperature. A hold time of 10 mins was provided before taking the measurements with the Agilent device. At room temperature, the resonance frequency was measured to be 160 MHz. As the heated DI water flows through the tubes placed under the Y5V capacitor, the capacitance started to decrease. This resulted in changes in the resonance frequency.

### 3.5.5 Experimental results

As shown in Figure 3.16, the heated circulating bath temperature was varied from 25 ℃ to 75 ℃. The resonance shift of ~4 MHz was observed for the temperature increase of 50 ℃. This experiment demonstrated the capability of the sensor to perform well with heated fluid flows which is like phenomena in the human body's blood circulation system. Therefore, this sensor can also be used as an implantable sensor if its size is further miniatured.
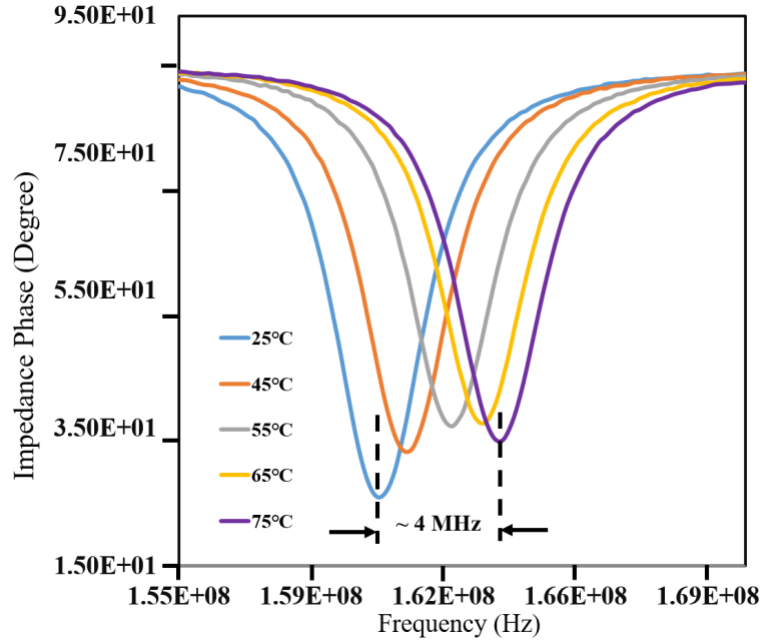
**Figure 3.16: Resonance changes in flow loop testing.**

## 3.6 Miniaturized passive wireless temperature sensor

For increasing the potential applications of the passive wireless sensor in implantable devices, shrinking its size is necessary. The fabrication expertise acquired in the fabrication of the larger device can be useful for the fabrication of this miniaturized device as well. The dimension of the miniaturized wireless temperature device targeted in this study was 6 mm$^2$, and thicker Cu-clad PI was used to achieve better results.

### 3.6.1 Design consideration

While designing the miniaturized sensor that is four times smaller than the previous larger coil, the parameters such as line width, line spacing, number of turns, and fill ratios are carefully considered. Increasing the dimensions of any of these parameters eventually increases the coil area and the resonant frequency range. Therefore, designing a coil with the desired resonant frequency

40

range and the coil area of ~5 mm$^2$ required the careful choice for each of the above-mentioned parameters.

Extensive studies have been performed on the effect of the coil resistance with the increase in the number of turns and the line width of planar inductor coil [17]. For example, have shown the increase in the number of turns results in an increase in the resistance of the coil, which results in a degraded Quality factor. Moreover, at higher frequencies, the current changes its path and starts flowing through the surface of the coil, which results in an uneven current redistribution between the coil turns. This phenomenon is known as the skin effect which leads to an increase in the coil resistance [17]. As shown in Figure 3.17, at higher frequencies the coil shows an increasing trend of resistance due to the skin effect. The increase in the number of turns and the fill ratio (line width) eventually increases the coil resistance, which leads to undesirable effects.

Therefore, the smaller coil as shown in Figure 3.18 is designed having seven turns, 175 µm line-width, and 210 µm line spacing. The theoretical value of the inductance of the miniaturized device was calculated to be 113 nH by using eq (2) and (3). As discussed, at higher frequencies the skin effect is more prominent. Therefore, to reduce this phenomenon the LC tank circuit was tuned for the lower frequency ranges by selecting the lower value of the Y5V capacitance (1 nF). Moreover, as discussed earlier the smallest value of the commercially available capacitance is 1 nF. Therefore, the 1nF Y5V commercial capacitor chip (Series 0805, AVX Co., SC, USA; dimensions 2.01×1.25×0.5 mm$^3$) was selected for designing the miniaturized device.
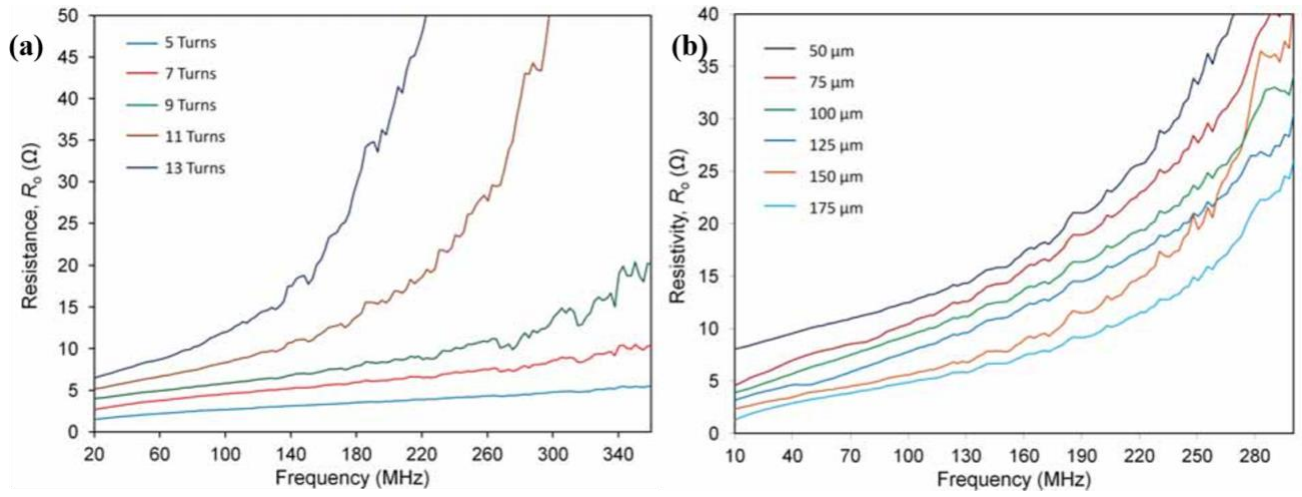
**Figure 3.17: Frequency dependent characteristics of the inductor coil (a) no. of turns; (b) line width [17].**
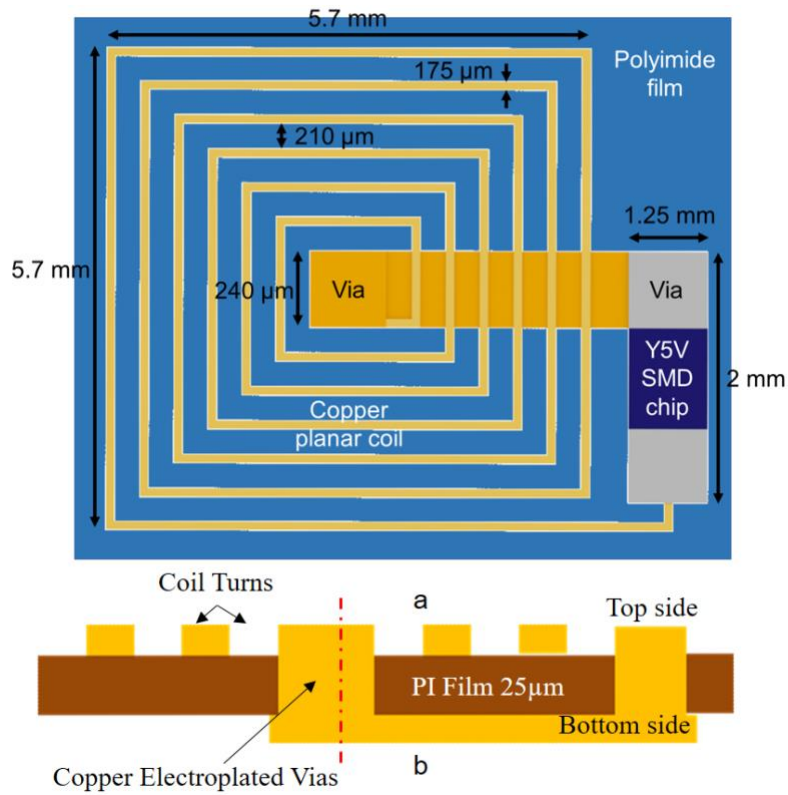


**Figure 3.18: Conceptual design of the fabricated wireless temperature sensor (a) top schematic view (b) schematic fabricated structure.**

### 3.6.2   Mask design

The new mask used for this device was designed using the widely used open-source K-layout software, and the CAD file was printed by a 3rd party vendor (Fineline Imaging, Inc. CO, USA) using 40 K dpi on 4'' extremely high contrast polyester-based photo mask. To achieve the high degree of flatness, this mask was later taped on 5'' clear glass slide before UV exposure.

**Table 3.3:Mask design parameters for the smaller coil**

| Parameter | Dimensions |
|---|---|
| Number of Turns | 7 |
| $D_{in}$ ($\mu$m) | 240 |
| $D_{out}$ (mm) | 5.7 |
| Line Width ($L_w$) ($\mu$m) | 175 |
| Line Spacing ($L_s$) ($\mu$m) | 210 |
| Coil Dimension (mm$^2$) | 5.7 x 5.7 |

### 3.6.3   Fabrication process

The miniaturized wireless passive sensor was also fabricated using the process flow shown in Figure 3.9. However, the materials used were different. The planar inductor coil was fabricated using a double-sided copper clad PI film from Dupont pyralux AP9111R 35-$\mu$m thickness in this effort to achieve better results by reducing the circuit resistance. Photolithography for the circuit fabrication was performed with the dry-film photoresist (30-$\mu$m thick Dupont Riston FX930).

The first step in the fabrication process was to form the capacitor electrode by wet-etching the copper clad layer on the back-side using the patterned FX930 photoresist and exposing it to UV for seven seconds. Next, the PI film was etched using the KOH-based solution to create two via-contact holes in the film. Then, the PI etching of the copper electroplating in the patterned FX930 photoresist mold was performed in a sulfuric acid-based bath at a current density of 20.2 mA/cm$^2$ for 80 mins, which filled the contact vias completely. The sample was coated again with the FX930 photoresist on both sides. Next, the inductor coil with seven turns was formed by wet-etching the copper clad layer on the front side and a UV exposure of nine seconds. The fabricated coil was then dried using the air gun, and the 1-nF Y5V commercial capacitor chip was manually bonded onto the two terminals of the inductor using Chemtronics CW2400 conductive epoxy; this was allowed to cure on the hot-plate for one hour at 100 ℃. The fabricated miniaturized wireless sensor is shown in Figure 3.19.
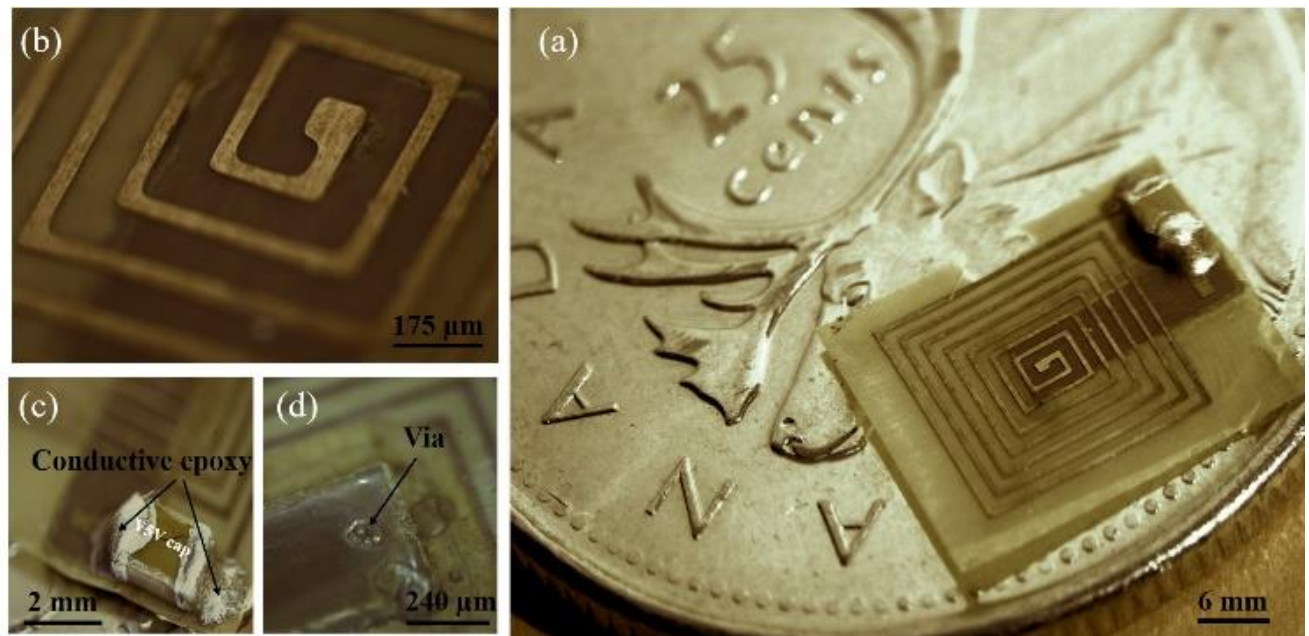


**Figure 3.19: (a) Fabricated smaller sensor device (~ 6mm): (b) Fabricated coil turns of line width 175 um: (c) Y5V mounted capacitor: (d) Electroplated vias on backside.**

### 3.6.4    Experimental setup and characterization

The experimental setup for tracking the frequency shift, as shown in Figure 3.20,  used a Peltier heater CP20251 (dimensions 20x5.1 mm and 2A INP) as the heating device and the Agilent network analyzer for monitoring the changes in the resonant frequency due to the heat [38]. The fabricated wireless sensor was glued onto the Peltier heater using polyamide tape such that the bottom side of the wireless sensor was touching the hot junction. The HP 6632A DC power supply was used to supply the required constant voltage of Vmax= 8.6V and the variable current to the Peltier heater; this achieved the desired temperature on the hot junction.
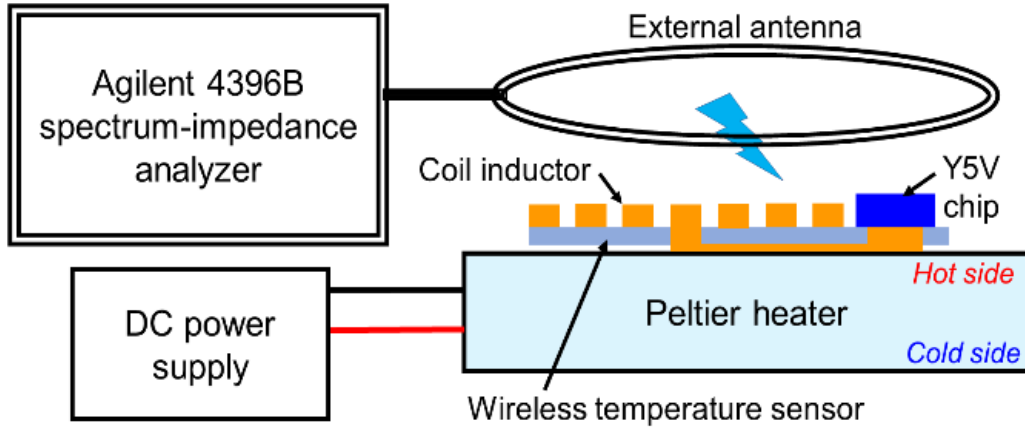


**Figure 3.20: Experimental setup for the detection and testing of the miniaturized sensor**

### 3.6.5    Results and discussion

The fabricated miniaturized wireless temperature sensor was characterized using the setup discussed in Section 3.6.4. The fabricated coil inductance was measured to be 120 nH; this was close to the theoretical calculated value of 113 nH, using eq (3) and eq (4). The total resistance of the wireless sensor was measured to be $2.5\Omega$ using the digital multimeter. The Q-factor was measured to be 14 which is lower than the larger sized fabricated sensor. The measured

45

temperature response of the fabricated wireless sensor is shown in Figure 3.21. By using eq (1) and the capacitance value of 1 nF, the calculated theoretical value of the resonance frequency is 14.97 MHz, whereas the measured value is 15.22 MHz at room temperature. Therefore, the measured value of the resonance frequency closely matches the theoretical value. The frequency shift was monitored for increased temperature of 13 ℃. A noticeable shift in the resonance frequency of ~1.5 MHz was observed between 27 ℃ to 40 ℃ as shown in Figure 3.21. It can be observed that the impedance phase dip of the measured coil decreased with as the temperature increased. This is possibly due to an increase in the coil resistance with the increase in temperature. The temperature co-efficient (α) of copper is +0.004041/℃ (at room temperature) which is related to the resistance of copper at room temperature. Therefore, an increase in temperature changes α which also increases the coil resistance. The new miniaturized prototyped wireless devices are tested to demonstrate their designed function, revealing frequency responses of 77-119 KHz/°C. It can be observed from Figure 3.22 that resonance frequency calculated using the theoretical value (measured C from section 2.6 and calculated L using eq (3) ) and the measured value closely matches with very low error. The results demonstrate an error between the measured and theoretical results of 3.9 % initially which gradually decreases to 2% with higher temperatures. This follows the trend discussed for the discrete and larger-coil devices.
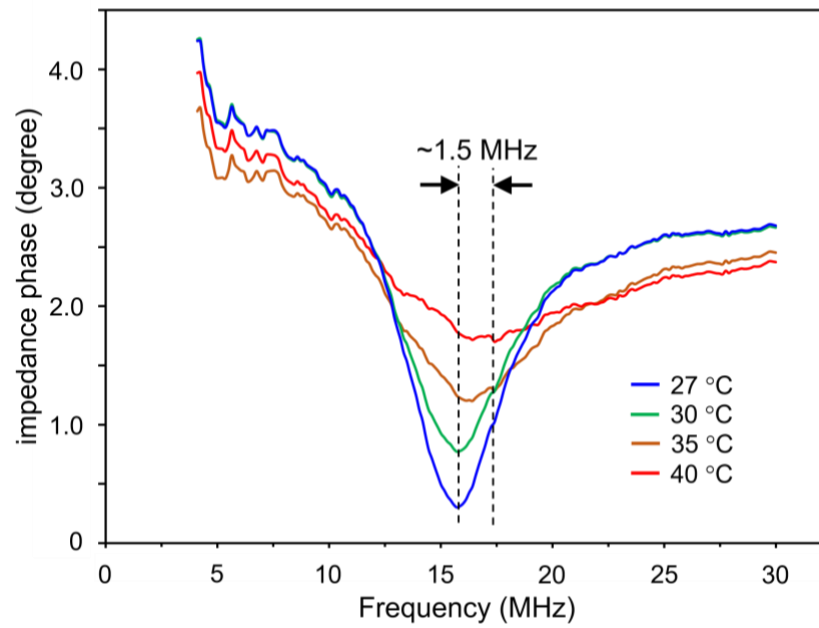
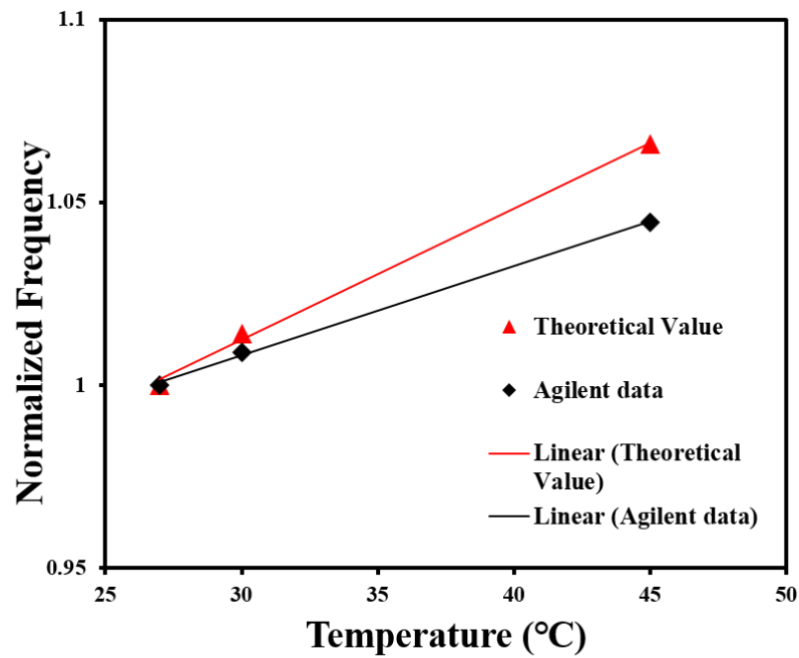**Figure 3.21: Measured temperature response of the resonant frequency of the ~6mm$^2$ device.**



**Figure 3.22: Comparison of the shift in the resonant frequency w.r.t temperature in the ~6 mm coil:**

**measured value (black) vs. theoretical value (red).**

47

## 3.7 Conclusion

A miniaturized version of a passive wireless temperature sensor has been designed, fabricated, and reported in this chapter. It was demonstrated that a commercial Y5V dielectric capacitor can be used as sensing element for the development of a low-cost /disposable wireless temperature sensor. The discrete device exhibited a frequency response of 116.66 KHz/℃. The larger fabricated sensor (~20 mm$^2$) demonstrated a frequency response between 106-150 KHz/℃ and the miniaturized fabricated device (6 mm$^2$) had a frequency response between 77-119 KHz/°C, with a decrease in capacitance of 8.25 pF/°C.

All of the experimental results were verified and validated with theoretical values. The fabricated sensor demonstrated a significant shift in the resonance frequency which can be used to estimate temperatures over surfaces. The device uses flexible circuit materials which further expands its application areas to wearable sensors. Table 3.4 provides a summary of the reviewed state of the art temperature sensors [2-16] [41]. The proposed larger and miniaturized fabricated wireless temperature sensor devices demonstrated a sensitivity of 106-150 KHz/℃ and 77-119 KHz/°C, respectively. Among all of the reported devices, the fabricated wireless temperature sensor has the smallest dimensions of 6 x 6 x 0.09 mm$^3$. In addition, this device has a low fabrication cost due to the minimal use of the clean room and the commercially available low cost Y5V capacitor in comparison to the other devices discussed in Chapter 2.

However, the impedance phase dip was significantly affected by an increase in temperature in the proposed device. This is due to changes in the temperature co-efficient of copper at higher temperatures. This change also increases the resistance of copper in the LC circuit, making the Q-

factor even lower. Hence, it becomes more challenging to track the shift in the resonance frequency

at temperatures above 40 ℃, which may limit it use in some applications.

**Table 3.4 Summary of passive wireless temperature sensors**

| Reference | Capacitance | Inductance | Materials | Dimensions | Sensitivity | Range (℃) |
|---|---|---|---|---|---|---|
| [12] | 0.24 nF | 0.68 µH | Ceramic | Diameter 28.5mm | --- | 0-235 |
| [2] | 22.1 pF | 255 µH | Si and Al | 50 x 50 x 0.63 mm$^3$ | 60fF/℃ | 30-330 |
| [13] | 11.76 pF | 1.348 µH | Ferro-electric ceramic | 36 x 36 x 0.68 mm$^3$ | -5.75 KHz/℃, 16.67 KHz/℃ | 25-430, 430-700 |
| [2] | -- | ---- | Graphene Oxide | Diameter 10 mm | 59.3 KHz/℃, 46.1 KHz ℃ | -40 – 0, 0-60 |
| [2] | -- | ---- | Alumina Ceramic | 37 x 37 x 37 mm$^3$ | 2 KHz/℃ | 25-1000 |
| This work: Large planar device | 10 nF | 1.55 µH | Cu and PI | 20 x 20 x 0.06 mm$^3$ | 106-150 KHz/℃ | 23-100 |

| This work: Miniaturized planar device | 1 nF | 120 nH | Cu and PI | 6 x 6 x 0.09 mm$^3$ | 77-119 KHz/°C | 23-50 |
|---|---|---|---|---|---|---|

# Chapter 4: Development of a low-cost impedance analyzer

## 4.1 Motivation

Commercial impedance analyzers are instruments used for acquiring complex electrical impedance measurements, and they have a high cost (e.g. Agilent spectrum impedance analyzers > $30K). For our research, to expand the capabilities of the fabricated device, the development of a portable low-cost impedance analyzer was investigated. Moreover, impedance measurements can also help to track temperature changes using our wireless fabricated sensor. The portable, low-cost analyzer provides an alternative to bulky and expensive impedance/Network analyzers, which are not well-suited for use in environments such as an intensive care unit. Here, an analyzer is proposed that uses a Digilent  PmodIA impedance analyzer PCB along with a single-board computer such as Raspberry Pi 3.

## 4.2 Digilent pmodIA impedance analyzer

The Digilent  PmodIA  is small size (4.1 cm x 2.0 cm) PCB using the analog device AD5933, a 12-bit impedance converter [38]. It offers programmable frequency sweep with a built-in programmable gain amplifier. Figure 4.1 shows the PmodIA chip. It consists of 2x4-pin ports with I$^2$C interfaces. The AD5933 has an onboard frequency generator and an analog-to-digital (ADC) converter; it is capable of exciting external unknown impedance at known frequencies. These known frequencies are then sent out through one of the two SMA (Sub Miniature version A) connectors with a 50 Ω impedance. The frequency response is later captured by a second SMA connector and sent to the ADC, Here, a discrete Fourier transform (DFT) is performed on sampled data and the real and imaginary parts of the frequency response are stored in on-chip data registers.

The magnitude of the unknown impedance as well as the relative phase of the impedance at each point in the generated frequency sweep can be calculated from these registers [38].
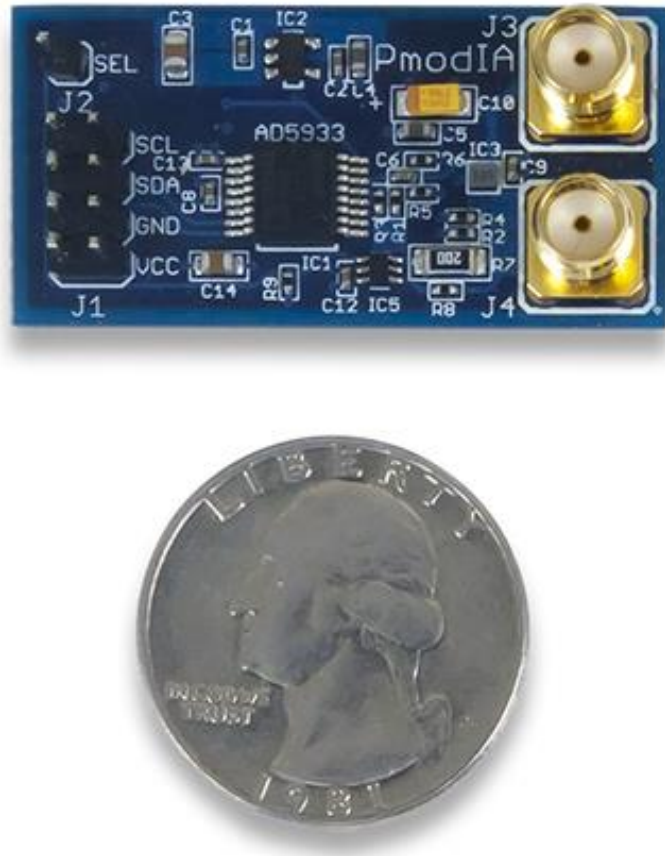


**Figure 4.1: Digilent PmodIA PCB schematic [38].**

## 4.3 Experimental setup

The complete impedance analyzer setup is shown in Figure 4.2 and Figure 4.3. It consists of Raspberrypi 3 (Single board computer), Digilent PmodIA, breadboard, SMA connector, external single loop antenna, and a monitor. The Raspberrypi is interfaced as the master device, and the PmodIA as the slave device in the configuration. The Raspberrypi running Raspbian Os and WiringPi library is installed for enabling $I^2C$ communication between Rasperrypi 3 and PmodIA

PCB. Moreover, a discrete LC resonator was developed with a resonant frequency of 1.01 MHz for the functional validation of the analyzer. The breadboard is used for mounting the SMA connectors, which is connected to external antenna. This external antenna is then aligned with the discrete LC resonating circuits. The SMA connectors having external antenna and the LC resonating circuits have a separation distance less than 2 cm.
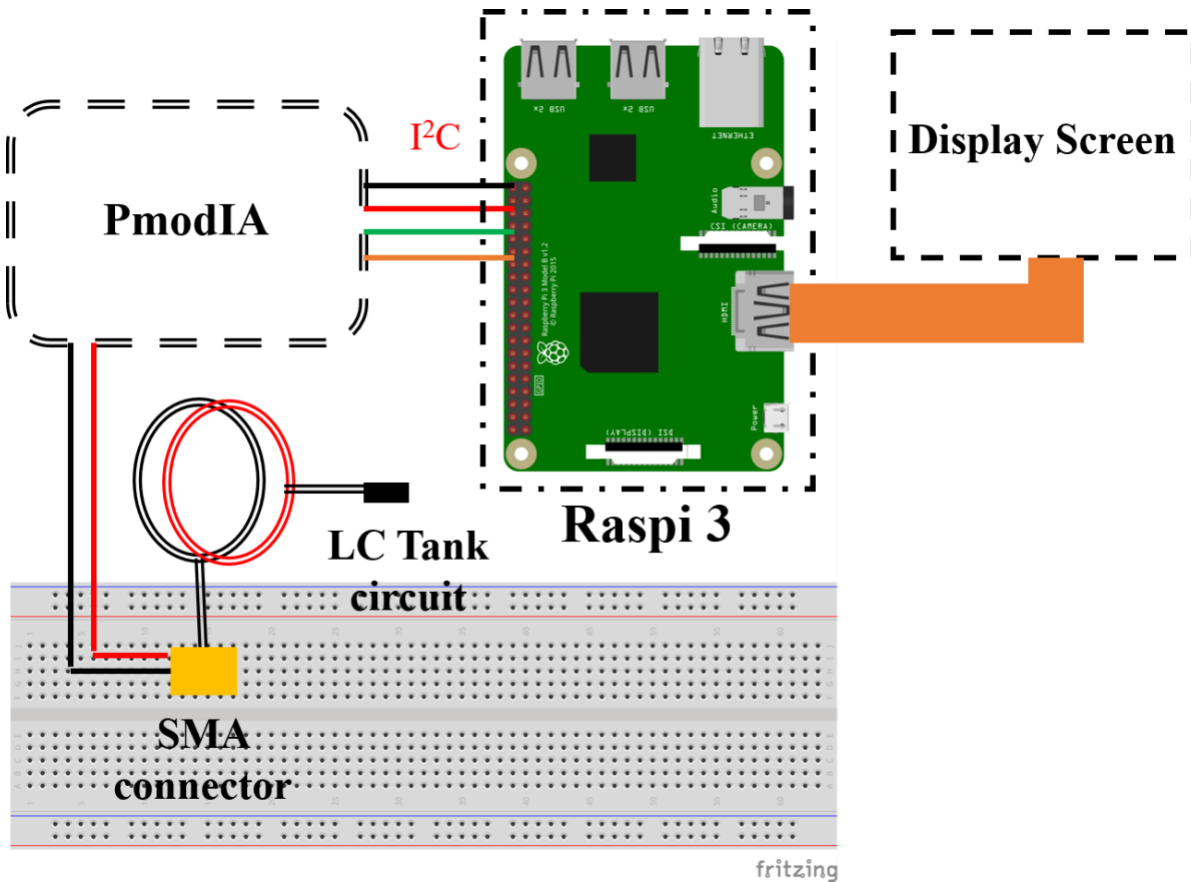


**Figure 4.2: Illustrative Experimental setup for the low-cost Impedance Analyzer**
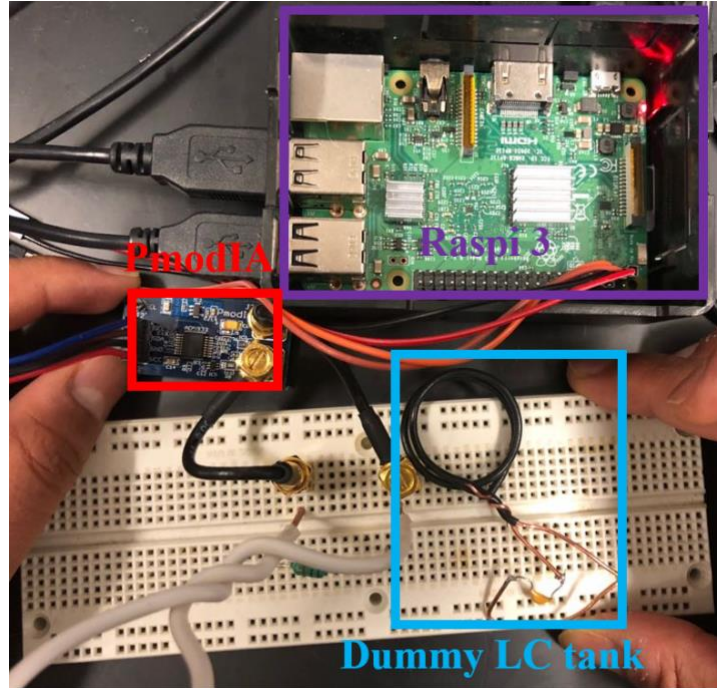
**Figure 4.3: Actual experimental setup for the low-cost Impedance analyzer.**

## 4.4 Frequency sweep

PmodIA allows the user to perform a frequency sweep over a range of frequencies to determine the impedance characteristics of circuit. As discussed in the previous section, the $I^2C$ interface was established between Raspberrypi 3 and PmodIA. Three parameters were provided by the user to perform the frequency sweep: starting frequency, increment frequency value after each step, and the number of steps in a sweep. This information is then stored in two 24-bit words and one 9-bit word respectively. Moreover, the user must also provide the peak-to-peak voltage of the output frequency in a sweep by setting bits 10 and 9 in the control register. Once the circuit has been excited, it takes some time to reach a steady state. The user can also program the settling time for each point in a frequency sweep. A C-program was used to provide all of the input parameters from the user and provided the calculated hexadecimal values for each control register to the

54

AD5933 IC [38]. The frequency sweep parameters used for our measurements are shown in Figure 4.4.



**Figure 4.4: User defined Frequency Sweep parameters**

## 4.5 Impedance calculations

The electrical impedance consists of both real and imaginary numbers. The impedance equation can be express as shown in equation [38].

$$Z = Real + j * Imaginary \tag{5}$$

where, $Real$ is the real component, $Imaginary$ is imaginary component, and $j$ is imaginary number (equivalent to $j = \sqrt{-1}$). In polar form, the impedance can be expressed as:

$$Impedance = |Z| \angle \theta$$

where, $|Z|$ is the magnitude and $\angle \theta$ is the phase angle.

$$|Z| = \sqrt{Real^2 + Imaginary^2}$$

$$\angle\,\theta = tan^{-1}\frac{Imaginary}{Real} \tag{6}$$

The 12-bit analog-to-digital converter within the IC AD5933 (slave device) samples the frequency response from unknown impedances at up to 1 MSPS (million samples per second) for every point in the frequency sweep. Before storing the measurements, PmodIA performs aiscrete fourier transform (DFT) on the sample data; there are 1024 samples for each frequency step. The DFT results are stored in two separate registers having real and imaginary values. After each DFT computation the master device (Raspberrypi 3) reads these values from the real and imaginary registers [38-39].

## 4.6 Measurements and results

The goal in this step was to track the changes in impedance values using the low-cost analyzer and validating the results with Agilent impedance analyzer. To track the shift in resonant frequencies, the impedance was first measured using the Agilent spectrum analyzer and then measurements were made using the developed PmodIA based impedance analyzer. Then, the measurements results are compared. Therefore, in this experiment the inductance of the discrete LC circuit was varied (by manually modifying the shape of the loop coil of the circuit) while the capacitor was kept at fixed value. The change in the loop shape results in a change in the inductance value; this consequently changes its electrical impedance and resonating frequencies. The frequency response measurements are performed using a discrete circuit with a known resonant frequency of 1.25 MHz as shown in Figure 4.7(a). Before starting the measurements, the manufacturer recommends performing a calibration step. The calibration was performed with a 10kΩ resistor with a known impedance value. Using the C-program, the user entered the calibrated value, and the impedance

analyzer determined the frequency responses of the 10kΩ resistor and the calculate error. The next step would be replacing this load (10kΩ) resistor with our discrete sample and performing the frequency sweep as discussed in Section 4.4. The measured frequency response output would then be printed on the console, and the graph is automatically plotted for the impedance value and frequency sweep range. Each measurement was performed after modifying the inductor loop shape of the discrete LC tank circuit and then validated with measurement results from the Agilent network analyzer. The measurement setup is illustrated in Figure 4.5 and Figure 4.6. The inductance is modified by changing in the loop shape of the discrete LC tank circuit, and resulting phase (degree) change is then measured with the Agilent network analyzer and compared with the impedance (Ω) measurements using low-cost impedance analyzer as shown in Figure 4.7. The discrete LC tank circuit's normalized phase was measured using the Agilent network analyzer and the impedance was measured using the low-cost PmodIA impedance analyzer as shown in Figure 4.7(b). The highest impedance value observed using the low-cost impedance analyzer was 3.68 Ω at the input frequency of 1.25 MHz; the resonance frequency phase measured on the Agilent analyzer was 1.52 MHz as shown in Figure 4.7 (b).
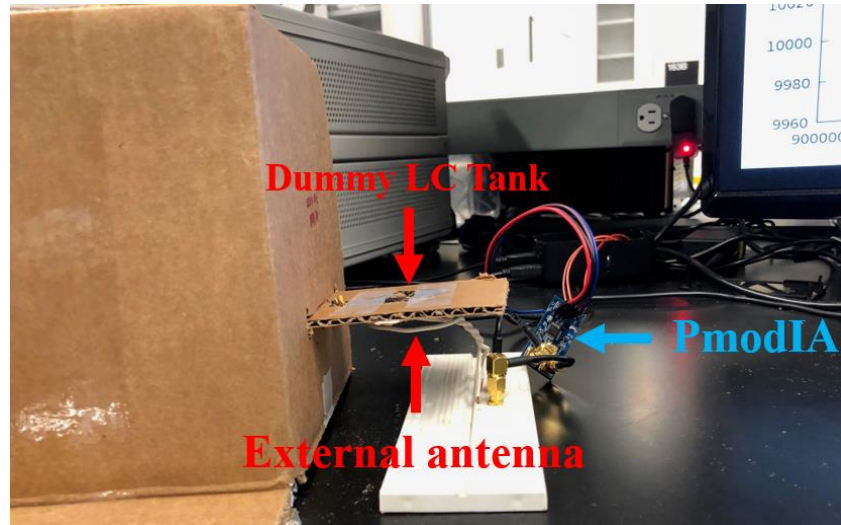
**Figure 4.5: Measurement setup for the low-cost impedance analyzer**
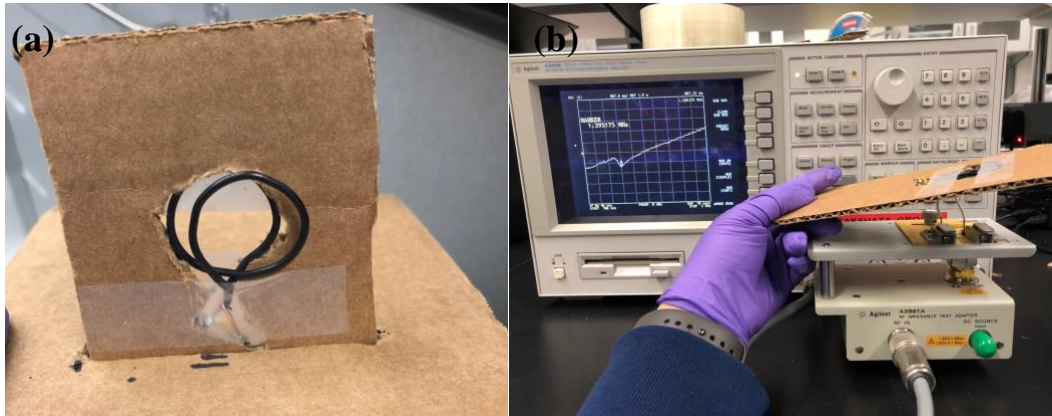


**Figure 4.6: Modifying inductance (a) Change in loop shape of the discrete LC circuit (b) frequency response of the modified loop shape discrete LC circuit.**
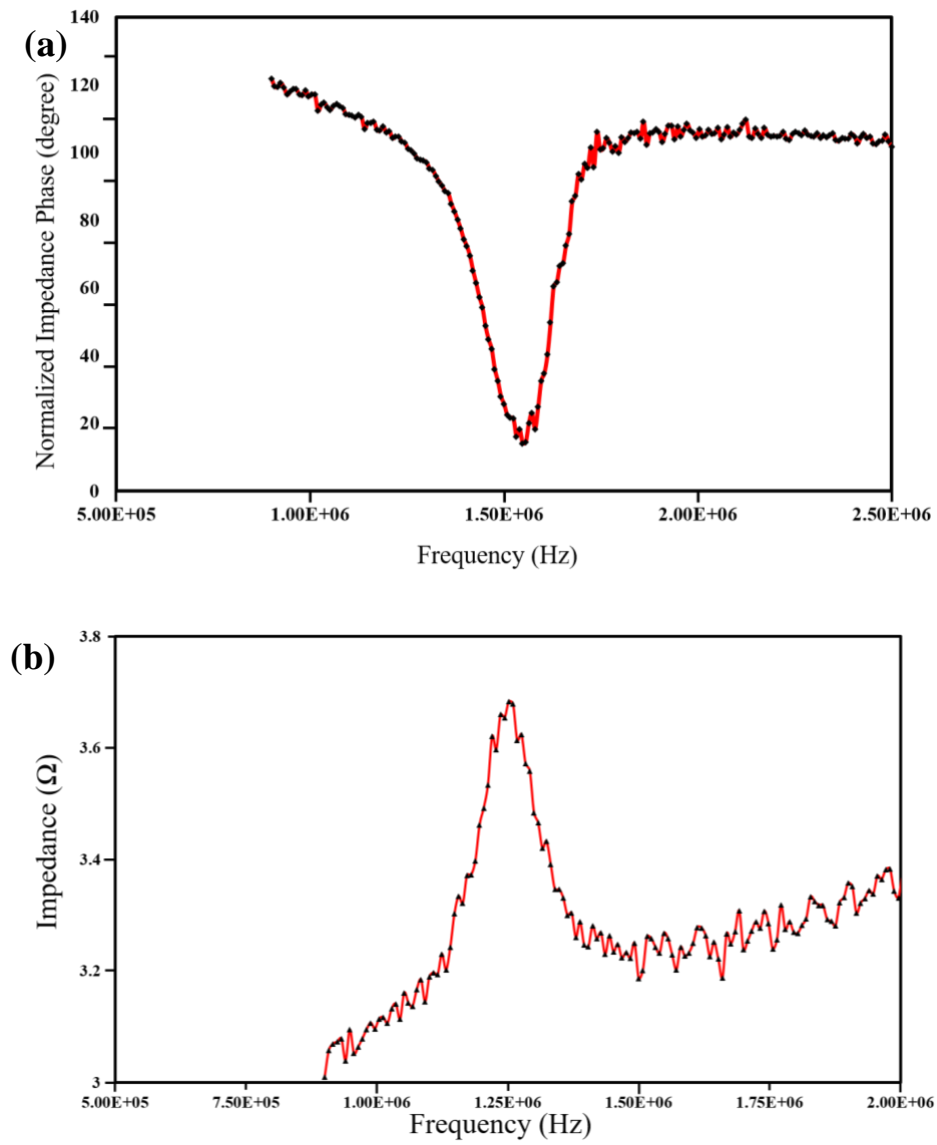
**Figure 4.7: Measurement results (a) Phase measurement using the Agilent network analyzer (b) Measured impedance using the low-cost impedance analyzer**
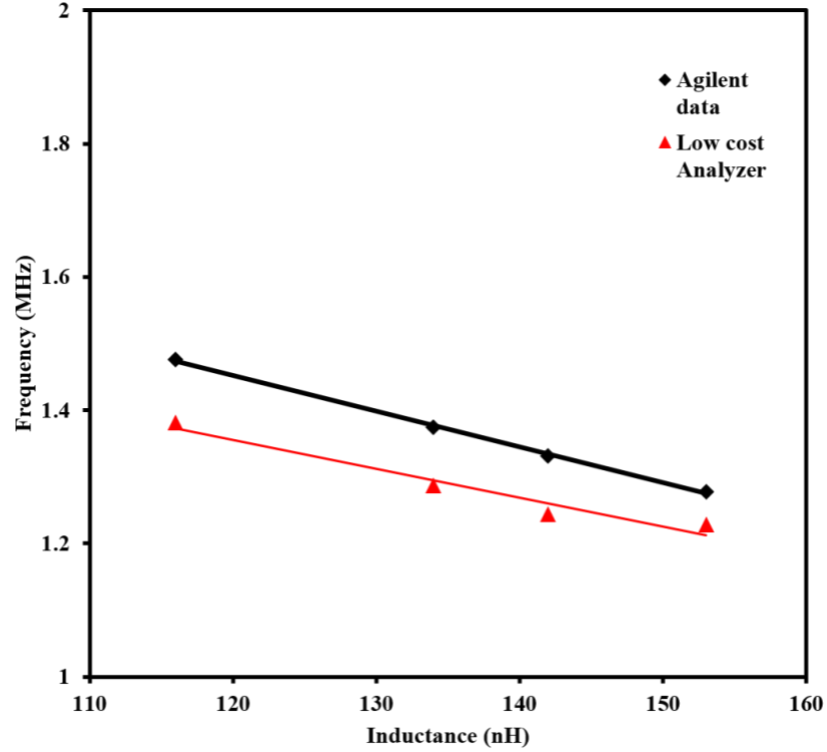
**Figure 4.8:Comparison of frequency responses (Agilent network analyzer and low-cost PmodIA based impedance analyzer).**

## 4.7    Conclusion

In this chapter, the development of a low-cost impedance analyzer using Digilent PmodIA (slave) and Raspi 3 (master) is demonstrated. The change in the frequency response is tracked and validated by comparing the measured impedance values and the phase dip of the same discrete sample using the developed analyzer with the highly sophisticated Agilent 4396B network analyzer. Moreover, the resulting shift in the frequency response due to changes in inductance values (modifying loop shape of the discrete sample) was tracked and compared with measurements using the low-cost analyzer and the Agilent network analyzer as shown in Figure 4.8. The error ~4% was determined between the measured values from the two analyzers. This

result suggests that the developed low-cost impedance analyzer is potentially promising for application to a portable LC-sensor reader through further improvement and optimization.

# Chapter 5: Conclusion and future work

This thesis presented the research results for investigating the design and development of passive wireless disposable temperature sensors and a low-cost impedance analyzer. This work investigated the in-depth characterization of Y5V based dielectric commercial capacitors, the design of wireless temperature sensors, and the fabrication of inductor coils with minimized clean-room usage. The application of this process to the design of flexible wireless passive temperature sensor was demonstrated.

## 5.1    Summary of research

A novel approach for fabricating disposable wireless temperature sensors with a rapid and low-cost inductor fabrication process, and the characterization of commercially available low-cost Y5V SMD capacitors are studied. The temperature dependencies of Y5V dielectric type SMD capacitor were studied at different frequencies ranges and considering their small footprints, two capacitor chips of 1000 pF and 10 nF were selected for the fabrication of the sensor. A discrete LC resonating circuit using the 1000 pF Y5V capacitor and a hand wound inductor of 10.44 µH was studied. The comparison of the theoretical and measured values demonstrated a good fit, with a low error of ~6 %.

This positive result encouraged for the development of passive miniaturized wireless temperature sensors using a flexible circuit technology. A novel fabrication process was used, involving a double-sided Cu-PI clad layer, wet-bench, and lithography processes. For early prototyping, a larger sized (~20 mm$^2$) temperature sensor was designed and good frequency responses of 106-150KHz/℃ were reported. However, for increasing its use to broader application areas, the

miniaturization of the sensor was performed using better materials such as high quality of mask and photoresist and thicker copper clad layer, with same fabrication processes. The miniaturized temperature sensor presented has a dimension of ~6 mm$^2$; it exhibited a good fabrication profile and a frequency response of 77-119 KHz/℃. The results were then compared and validated with the theoretical values; the observed errors for the discrete, large-coil, and miniaturized-coil devices were 5.2%, 18.3%, and 3.1% on average, respectively.

Furthermore, the development of low-cost impedance analyzer was presented which can be used as handheld device for tracking the changes in temperature wirelessly. The presented low-cost impedance analyzer uses Raspberry Pi and Digilent PmodIA PCB in a Master and Slave configuration. The frequency response of the Agilent network analyzer and the low-cost impedance analyzer are compared and validated with the theoretical values; the demonstrated error was ~ 4%.

## 5.2   Future work

There are two main directions for the future work. One of the main challenges encounter during the development passive wireless temperature sensor was low Q-factor. This can be improved by using thicker Cu-clad layer, lower capacitance value, higher inductance value (by increasing number of turns in coil) and minimizing contact resistance resulting in better Q-factor and signal to noise ratio. This process can also suitable for batch production of inductor coils which could increase the production rates up to three times.

Moreover, improvements in increasing functionality of low-cost Impedance analyzer including digital signal processing on frequency response of received signal from sensor, better integration of components on single handheld/portable system and development of continuous frequency response tracking/monitoring algorithm are important problems to investigate. In addition, establishing a more reliable connection between the temperature sensor and the monitoring device is also a subject of future work.

As the main objective of this research was to monitor temperatures wirelessly in diverse application domains (e.g., healthcare), conducting in-vivo tests would be an important, direction to explore. To this end, the device will need to be improved to be fully biocompatible. One approach to this improvement is conformal biocompatible coating of the device using Parylene C, a proven biocompatible polymer that have been used in the area of implantable devices [4].

# Bibliography

[1]     C. C. Collins, "Miniature Passive Pressure Transensor for Implanting in the Eye," *IEEE Transactions on Biomedical Engineering,* vol. BME-14, no. 2, pp. 74–83, Apr. 1967.

[2]     Q. Huang, L. Dong, and L. Wang, "LC Passive Wireless Sensors Toward a Wireless Sensing Platform: Status, Prospects, and Challenges," *Journal of Microelectromechanical Systems*, vol. 25, no. 5, pp. 822–841, Oct. 2016.

[3]     "(PDF) Passive Hybrid MEMS for High-Temperature Telemetric Measurements," *ResearchGate*.[Online].Available:

https://www.researchgate.net/publication/224096532_Passive_Hybrid_MEMS_for_High-Temperature_Telemetric_Measurements. [Accessed: 19-Apr-2019].

[4]     P. Chen, D. C. Rodger, S. Saati, M. S. Humayun, and Y. Tai, "Microfabricated Implantable Parylene-Based Wireless Passive Intraocular Pressure Sensors," *Journal of Microelectromechanical Systems,* vol. 17, no. 6, pp. 1342–1351, Dec. 2008.

[5]     B. Ando, S. Baglio, N. Savalli, and C. Trigona, "Cascaded 'Triple-Bent-Beam' MEMS Sensor for Contactless Temperature Measurements in Nonaccessible Environments," *IEEE Transactions on Instrumentation and Measurement*, vol. 60, no. 4, pp. 1348–1357, Apr. 2011.

[6]     Q. Ren, L. Wang, J. Huang, C. Zhang, and Q. Huang, "Simultaneous Remote Sensing of Temperature and Humidity by LC-Type Passive Wireless Sensors," *Journal of Microelectromechanical Systems,* vol. 24, no. 4, pp. 1117–1123, Aug. 2015.

[7]     "(PDF) A Novel Method to Read Remotely Resonant Passive Sensors in Biotelemetric Systems,"*ResearchGate.*[Online].Available:

https://www.researchgate.net/publication/3431242_A_Novel_Method_to_Read_Remotel
y_Resonant_Passive_Sensors_in_Biotelemetric_Systems. [Accessed: 19-Apr-2019].

[8]     "(PDF) Electrodeposited copper inductors for intraocular pressure telemetry,"
        *ResearchGate.*[Online].Available:

        https://www.researchgate.net/publication/228811503_Electrodeposited_copper_inductors
        _for_intraocular_pressure_telemetry. [Accessed: 19-Apr-2019].

[9]     M. Radovanovic, B. Mojic-Lante, K. N. Cvejin, V. V. Srdic, and G. M. Stojanovic, "A
        Wireless LC Sensor Coated with Ba0.9Bi0.066TiO3 for Measuring Temperature," *Sensors
        (Basel)*, vol. 15, no. 5, pp. 11454–11464, May 2015.

[10]    Y. Wang, Y. Jia, Q. Chen, and Y. Wang, "A Passive Wireless Temperature Sensor for
        Harsh Environment Applications," *Sensors (Basel)*, vol. 8, no. 12, pp. 7982–7995, Dec.
        2008.

[11]    Q. Tan et al., "A harsh environment-oriented wireless passive temperature sensor realized
        by LTCC technology," *Sensors,* vol. 14, no. 3, pp. 4154–4166, 2014.

[12]    T. Someya *et al.*, "Conformable, flexible, large-area networks of pressure and thermal
        sensors with organic transistor active matrixes," *PNAS*, vol. 102, no. 35, pp. 12321–12325,
        Aug. 2005.

[13]    J. Jeon, H.-B. Lee, and Z. Bao, "Flexible Wireless Temperature Sensors Based on Ni
        Microparticle-Filled Binary Polymer Composites," *Advanced Materials*, vol. 25, no. 6, pp.
        850–855, 2013.

[14]    S. E. Woodard, C. Wang, and B. D. Taylor, "Wireless temperature sensing using
        temperature-sensitive dielectrics within responding electric fields of open-circuit sensors

having no electrical connections," *Meas. Sci. Technol.*, vol. 21, no. 7, pp. 025107-1–025107-11, 2010.

[15] R. Kadefors, E. Kaiser, and I. Petersen, "Energizing Implantable Transmitters by Means of Coupled Inductance Coils," *IEEE Transaction on Biomedical Engineering*, vol. 16, pp. 177-183, 1969.

[16] B. Razavi, "RF MICROELECTRONICS Second Edition."

[17] C. Brasselet et al., "Effect of local heating on restenosis and in-stent neointimal hyperplasia in the atherosclerotic rabbit model: a dose-ranging study," Eur. Heart J., vol. 29, no. 3, pp. 402–412, Jan. 2008.

[18] C. Li et al., "Review of Research Status and Development Trends of Wireless Passive LC Resonant Sensors for Harsh Environments," *Sensors,* vol. 15, no. 6, pp. 13097–13109, Jun. 2015.

[19] Balanis C A 2005 *Antenna Theory: Analysis and Design* 3rd edn (New York: Wiley-Interscience) pp 170–8

[20] Wilson et al., "Y5V dielectric composition," United States Patent 5604167, Feb. 18th, 1997.

[21] "(PDF) Implantable Devices: Issues and Challenges," ResearchGate. [Online]. Available: https://www.researchgate.net/publication/276035384_Implantable_Devices_Issues_and_ Challenges. [Accessed: 19-Apr-2019].

[22] S. Scott, A. Kovacs, L. Gupta, J. Katz, F. Sadeghi, and D. Peroulis, "Wireless temperature microsensors integrated on bearings for health monitoring applications," in Proc. 24th IEEE *Int. Conf. Micro Electro Mech. Syst.,* Cancún, Mexico, Jan. 2011, pp. 660–663.

[23] M. S. Mohamed Ali, "Integration and wireless control methods for micromachined shape-memory-alloy actuators and their MEMS applications," T, University of British Columbia, 2012

[24] R. A. Groves, and N. D. Zamdmer, J.- Plouchart, R. A. Wachnik, and and, "Frequency-independent equivalent-circuit model for on-chip spiral inductors," *IEEE Journal of Solid-State Circuits,* vol. 38, no. 3, pp. 419–426, Mar. 2003.

 [25] S. S. Mohan, M. M. Hershenson, S. P. Boyd, and T. H. Lee, "Simple Accurate Expressions for Planar Spiral Inductances*," IEEE Journal of Solid-State Circuits*, 34(10), pp. 1419-1424, 1999.

[26] H. A. Wheeler, "Simple Inductance Formulas for Radio Coils," *Proceeding IRE*, Oct. 1928, vol. 16(10), pp. 1398-1400.

[27] V. Sridhar, "A micromachined Inductive Sensor using Folded Flex-Circuit Structures and its Wireless Telemetry Applications," *Master's thesis,* University of British Columbia, Vancouver, Canada, 2008.

[28] S. Brugger and O. Paul, "Field-Concentrator-Based Resonant Magnetic Sensor With Integrated Planar Coils," *Journal of Microelectromechanical System*, vol. 18(6), pp. 1432-1441, 2009.

[29] A. Eroglu, "Planar Inductor Design for High Power Applications," *Progress In Electromagnetics Research B*, vol. 35, pp. 53-67, 2011

[30] Z. Li, Z. Zhang, Q. He, Y. Fu, J. Zhao, B. Han, S. Li, J. Lan, and C. Li, "A Compensation Method to Measure the Mutual Inductance at Low Frequency," *IEEE Transaction of Instruments and Measurement*, vol. 60(7), pp. 2292-2297, 2011.

[31] D. R. Patrick and S. W. Fardo, *Electricity and Electronics Fundamentals*, 2nd Edn.

Fairmount Press, GA, USA, 2008.

[32]  M. S. Mohamed Ali and K. Takahata, "A Wirelessly Controlled Shape-Memory-Alloy MEMS Gripper Microfabricated using an Electroplating-Based Bonding Process," Solid-State Sensors, Actuators and Microsystems Workshop, Hilton Head, SC, USA, June 6-10, 2010, pp. 396-399.

[33]  Sajeeda and T. J. Kaiser, "Passive Telemetric Readout System*,*" *IEEE Sensors Journal*, vol. 6(5), pp. 1340-1345, 2006.

[34]  Y. K. Kim, E. Y. Kim, S. W. Kim, and B. K. Ju, "Low Temperature Epoxy Bonding for Wafer Level MEMS packaging," Sensors and Actuators A physical, vol. 143, pp. 323-328, 2008

[35]  P. Sample, T. Meyer, and J. Smith, "Analysis, Experimental Results, and Range Adaptation of Magnetically Coupled Resonators for Wireless Power Transfer*,*" *IEEE Transaction on Industrial Electronics*, vol. 58(2), pp. 544-554, 2011.

[36]  S. F. Pichorim and P. J. Abatti, "A Novel Method to Read Remotely Resonant Passive Sensors in Biotelemetric Systems," *IEEE Sensors Journal*, vol. 8, no. 1, pp. 6–11, Jan. 2008.

[37]  CUI INC., "Peltier Application Note," 2016.

[38]  Digilent, "PmoadIA Reference Manual," April 15th, 2016.

[39]  Analog Devices, "1 MSPS, 12-Bit Impedance Converter Network Analyzer," AD5933 datasheet Rev. F 2017

[40]  M. J. Madou, Manufacturing Techniques for Microfabrication and Nanotechnology, 3rd ed., vol. II, New York: CRC Press, 2011.

[41]  C. Li, Q. Tan, W. Zhang, C. Xue, and J. Xiong, "An embedded passive resonant sensor

using frequency diversity technology for high-temperature wireless measurement*," IEEE Sensors Journal*, vol. 15, no. 2, pp. 1055-1060, Feb 2015.